Treatment of hydrophobic polycyclic aromatic hydrocarbons and toxicity using GO-TiO₂-Sr(OH)₂/SrCO₃ nanocomposite via photocatalytic degradation

RUKİYE ÖZTEKİN [a, *], DELİA TERESA SPONZA [a]
[a] Department of Environmental Engineering
Dokuz Eylül University
Tınaztepe Campus, 35160 Buca/Izmir,
TURKEY

Abstract: - In this study, the effects of increasing sun light irradiation time (30 min, 120 min, 240 min and 360 min), increasing photocatalytic power (10 W, 50 W and 100 W), increasing graphene oxide (GO) nanoparticle concentrations (2 mg/l, 4 mg/l and 8 mg/l), increasing titanium dioxide (TiO₂) nanoparticle concentrations (1 mg/l, 3 mg/l, 6 mg/l and 9 mg/l), increasing GO-TiO₂-Sr(OH)₂/SrCO₃ nanocomposite concentrations (1 mg/l, 2 mg/l and 4 mg/l) on the destructions of four hydrophobic polycyclic aromatic hydrocarbons (PAHs) in a real petrochemical industry wastewater in Izmir (Turkey) were investigated. The yields in more hydrophobic PAHs with high benzene rings [benzo[*a*]pyrene (BaP) and benzo[*k*]fluoranthene (BkF)] were as high as the less hydrophobic PAHs with lower benzene rings [acenaphthylene (ACL) and carbazole (CRB)]; at pH=7.0, at 22ºC after 360 min sun light irradiation time, respectively. Maximum 97%ACL, 98%CRB, 98%BaP and 99%BkF PAHs removals was detected at 4 mg/l GO-TiO₂-Sr(OH)₂/SrCO₃ nanocomposite concentration, under 100 mW/cm² sun light intensity, at 100 W photocatalytic power, at 360 min sun light irradiation time, at pH=7.0 and at 22ºC, respectively. The effective PAHs concentrations caused 50% mortality in *Daphnia magna* cells increased from initial EC₅₀=342.56 mg/l to EC₅₀=631.05 mg/l, at pH=7.0 and at 22ºC after 360 min photocatalytic degradation time resulting in a maximum acute toxicity removal of 99.99%, at 4 mg/l GO-TiO₂-Sr(OH)₂/SrCO₃ nanocomposite concentration. The *Daphnia magna* acute toxicity was significantly reduced.

Key-Words: - *Daphnia magna* acute toxicity; graphene oxide; GO-TiO₂-Sr(OH)₂/SrCO₃ nanocomposite; petrochemical industry wastewater; photocatalytic degradation; polycyclic aromatic hydrocarbons; titanium dioxide.

1 Introduction

Polycyclic aromatic hydrocarbons (PAHs) are an important class of persistent organic pollutants (POPs), and have been ubiquitously found in the environment, [1]. Besides the natural sources, PAHs are often from anthropogenic sources such as incomplete combustion of fossil fuels, and accidental spillages of crude and refined oils, [2, 3]. Due to their persistence and potential harmful impact on the ecosystem and human health, PAHs have been classified as priority pollutants by the United States Environmental Protection Agency (USEPA), [4].

Wastewater treatment plants, especially those serving industrial areas, consistently receive complex mixtures containing a wide variety of organic pollutants. Groups of compounds present in the petrochemical industries include polycyclic aromatic hydrocarbons (PAHs), which are listed as US-EPA and EU priority pollutants, and concentrations of these pollutants therefore need to

be controlled in treated wastewater effluents, [5]. PAHs are ubiquitous environmental pollutants with mutagenic properties, which have not been included in the Turkish guidelines for treated waste monitoring programs, [6]. Several hydroxy-PAHs such as hydroxylated derivatives of Benzo[a]pyrene (BaP) and Chrysene (CHR) have been shown to possess estrogenic activity and cause damage to DNA leading to cancer and possibly other effects, [6, 7]. As a consequence of their strongly hydrophobic properties and their resistance to biodegradation, PAHs are not always quantitatively removed from wastewaters by activated sludge treatments, which very efficiently relocate them into treated effluents.

Titanium dioxide (TiO₂) is the most used photocatalyst due to its environment friendliness, abundant supply and cost-effectiveness, [8]. However, due to the wide bandgap (3.2 eV for anatase and 3.0 eV for rutile), [9], TiO₂ can only be excited in the ultraviolet (UV) range, which

accounts for only 4% of the solar radiation, [10]. Therefore, various efforts have been attempted to extend the utilization of TiO_2 to the visible light range ($> 40\%$ of the solar energy), such as metal/non-metal doping, noble metal deposition, semiconductors coupling, and photosensitization, [11, 12].

Graphene is a flat monolayer of carbon atoms tightly packed into a two-dimensional honeycomb lattice. In recent years, graphene has attracted a great deal of attentions for its potential applications in many fields, such as nano-electronics, fuel-cell technology, supercapacitors, and catalysts, [13, 14]. Graphene oxide (GO) is one of the most important precursors of graphene, and thus, they share similar sheet structures and properties such as high stability and semiconducting characteristics, [10, 15]. GO can enhance the light absorption via expanding the photo-responsive range to visible light and suppress the charge recombination by serving as a photo-generated electron transmitter, when coupled with TiO_2 , [10]. To further enhance the conductivity and reduce the bandgap, noble metals (e.g., gold, palladium and platinum) are often incorporated to the GO-TiO_2 nanocomposite by surface deposition, [10, 16].

Compared with noble metals, strontium (Sr), as an alkaline earth metal, has much wider and richer sources, and it is the 15th most abundant element in the Earth's crust with an estimated abundance of nearly 360 mg/l, [17]. Sr has been widely employed as a dopant for various semiconductors (e.g., TiO_2, zinc oxide and germanium dioxide) to enhance the photocatalytic activities, [18]. Moreover, the OH and carbonate forms of Sr ($Sr(OH)_2$/$SrCO_3$) have been reported to have high photocatalytic activity under visible-light irradiation, [19-21].

The reactive oxygen species (ROS) formed during TiO_2 photocatalysis include the hydroxyl radical ($OH^{\bullet}$), superoxide anion radical ($O_2^{-\bullet}$), hydroperoxyl radical ($HO_2^{\bullet}$), singlet oxygen ($^1O_2$), and their subsequent reactions with the target contaminants occur at or very near the TiO_2 surface, [8, 22]. $OH^{\bullet}$ radicals, generated on the surface of the catalyst following oxidation of water from the positive holes of TiO_2, are non-selective oxidizing species with strong oxidation potential (2.80 V) that rapidly react with most organic compounds with rate constants in the order of 10^6 - 10^{10} 1/M.s, [23]. Various studies have investigated the degradation of MC-LR in pure solutions or crude extracts with TiO_2 photocatalysis to study the effect of specific water quality parameters, [24-27], or the properties of the photocatalyst used, [24, 28-32]. Solar light activated materials have also been tested to reduce

application cost, [27-29, 30, 33, 34]. Herein, sulfate radical generating oxidants were added as a way to reduce the energy requirements of the photocatalytic system for the removal of MC-LR as most of the light activated materials are not currently mass produced. Sulfate radicals ($SO_4^{-\bullet}$) are among the strongest oxidants known for the abstraction of electrons (2.5 V - 3.1 V), [35, 36]. They are much stronger than $OH^{\bullet}$ radicals (1.89 V - 2.72 V), [23], and other commonly used in the drinking water industry oxidants, such as permanganate (E=1.70 V), [37], and hypochlorous acid (E=1.49 V), [38]. $SO_4^{-\bullet}$ radicals can be produced through homolytic dissociation of the oxidants through heat and radiation and e^- transfer mechanisms from Fenton-like reagents, [39-41]. Neta et al., [36], reported that owing to their selectivity, $SO_4^{-\bullet}$ radicals are more efficient oxidants for the removal of organic compounds with unsaturated bonds and aromatic constituents than the $OH^{\bullet}$ radicals. Yet there are limited studies on $SO_4^{-\bullet}$ based AOPs (compared with $OH^{\bullet}$) for the degradation of recalcitrant organic contaminants and especially cyanotoxins, [41-44]. Even fewer studies have investigated the effect of coupling $SO_4^{-\bullet}$ radical generating oxidants with TiO_2 on the removal of emerging contaminants with various light sources. Furthermore, simulated solar irradiation (SSI) has been used in the SSI/TiO_2/PS treatment, [45], and showed higher potential for the removal of the pesticide DEET compared with the SSI/TiO_2/H_2O_2 system. PS was also coupled with TiO_2 photocatalysts for the degradation of dyes under solar, [46], and UV radiation, [47].

The aim of this study was to examine the effects of increasing GO-TiO_2-$Sr(OH)_2$/$SrCO_3$ concentrations (1 mg/l, 2 mg/l and 4 mg/l), increasing GO concentrations (2 mg/l, 4 mg/l and 8 mg/l), increasing TiO_2 concentrations (1 mg/l, 3 mg/l, 6 mg/l and 9 mg/l), increasing photocatalytic powers (10 W, 50 W and 100 W) and increasing sun light irradiation times (30 min, 120 min, 240 min and 360 min) on the photocatalytic degradation of four hydrophobic PAHs namely ACL, CRB, BaP and BkF in a real petrochemical industry wastewater, at pH=7.0 and at 22°C, respectively. Furthermore, the effects of the operational conditions in a real petrochemical industry wastewater on the removal of acute toxicity were also determined using *Daphnia magna.*

2. Materials and Methods

2.1. Material Synthesis

GO was synthesized according to the modified Hummers method, [48], and titanium dioxide nanoparticles (Nano-TiO$_2$) were prepared following the approach reported in Xu et al., [49]. Supporting Information (SI) Text S1 provides detailed procedures for the preparation of GO and Nano-TiO$_2$. The GO-TiO$_2$ nanocomposite was then synthesized through the sono-chemical reaction of Nano-TiO$_2$ in the presence of the GO, [15]. In brief, 3 g of the mixture of GO and Nano-TiO$_2$ (mass ratio=2/1) was added to 100 ml of distilled water, and stirred for 0.5 h at room temperature (22±1°C). The suspension was then sonicated for 1 h. The resultant composite was recovered by filtration, rinsed with ethanol and then freeze-dried to yield the GO-TiO$_2$ composites. Subsequently, dispersing known mass of GO-TiO$_2$ (30 wt% of the final mass) in a 500 ml of sodium hydroxide (NaOH) solution (1 M), and a pre-determined amount of strontium chloride (SrCl, 0.5 M) was added dropwise to the dispersion at a rate of 2.0 ml/min using a Titronic Universal titrator (SCHOTT, Mainz, Germany). The resulting material, GO-TiO$_2$-Sr(OH)$_2$/SrCO$_3$, was then filtered, washed with distilled water until no chloride was detected in the washing water, and then freeze-dried for 48 h. For comparison, a GO-Sr(OH)$_2$/SrCO$_3$ nanocomposite was also prepared by the similar procedure with 20 wt% GO but without TiO$_2$.

2.2. Material Characterization

The X-ray diffraction (XRD) measurements were performed on a PW1820 X-ray diffractometer (Philips, Amsterdam, Netherlands) using Cu Kα radiation. Scanning electron microscopy (SEM) images were obtained with a JSM-840A electron microscope (JEOL, Tokyo, Japan) equipped with energy dispersive X-ray (EDX) micro-analytical system (EDAX, Mahwah, NJ, USA). The EDX analysis was performed at -263.15°C magnification to map the distribution of Sr and Ti on the nanocomposite surface. Fourier transform-infrared (FTIR) measurements were carried out with a Nicolet 560 FTIR spectrometer on KBr wafers (Thermo Fisher Scientific Inc., MA, USA). The spectra were recorded from 4000 1/cm to 400 1/cm at a resolution of 4 1/cm. Nitrogen (N$_2$) adsorption-desorption isotherms were measured using AS1Win (Quantachrome Instruments, FL, USA) at the liquid N$_2$ temperature of -196.15°C, from which Brunauer-Emmett-Teller (BET) specific surface area (S$_{BET}$), micropore volume (V$_{mic}$), total pore volume (V$_t$),

and pore size distribution (PSD) were derived. Potentiometric titration measurements were carried out with a T50 automatic titrator (Mettler Toledo, Columbia, MD, USA) and the total surface charge (Q$_{surf}$, mmol/g) of the nanocomposite was then calculated. Differential thermal gravimetric (DTG) analysis was conducted on an STA449F3 instrument (Netzsch, Selb, Germany). Reactive oxydizing agents such as potassium peroxymonosulfate (PMS, HSO$_5^-$), potassium persulfate (PS, K$_2$S$_2$O$_8$), and the quenching agent sodium thiosulfate (Na$_2$S$_2$O$_3$) were purchased from Sigma-Aldrich (Poole, UK).

2.3. Photocatalytic Degradation

Simulated sun light was generated using a 94041A solar simulator (Newport Corporation, Irvine, CA). A cylindrical quartz tank reactor with a Pyrex pillar (80×70 mm) was fabricated as the photoreactor. The light intensity reached the reactor was 100 mW/cm^2. The detailed information on the solar simulator and photoreactor has been reported elsewhere, [50]. PAHs were purchased from Alfa Aesar (Ward Hill, MA, USA), and a stock solution of 2 g/l was prepared in methanol. Deionized (DI) water (Millipore Co., 18.2 MΩ·cm) was used in preparing all aqueous solutions. Typically, the photocatalytic degradation kinetic tests were conducted under the following conditions: solution volume=250 ml, initial PAHs concentration=1 mg/l, 5 mg/l and 10 mg/l, catalyst dosage=50 mg/l, pH=7.0±0.2, and T=22±1°C, respectively. The solution-photocatalyst mixture was first stirred in the dark for 2 h to allow PAHs adsorption to reach equilibrium. Subsequently, photodegradation was initiated by exposing the reactor to the simulated sun light.

2.4. Analytical Methods

UV–Visible spectra of solutions were obtained using an HP 8453 UV–Vis spectrophotometer (Agilent Technologies, Santa Clara, CA, USA). PAHs concentration was determined using an HP 1100 HPLC system (Agilent Technologies, Santa Clara, CA, USA) with a detection limit of 2.5 μg/l at the UV detection wavelength of 250 nm. Photodegradation intermediates were analyzed using an HP7890A/HP5975C gas chromatography-mass spectrometry (GC–MS) system (Agilent Technologies, Santa Clara, CA, USA).

The contributions of various reactive oxygen species (ROS) during the photocatalytic degradation process were investigated by adding scavengers to selectively quench radicals; i.e., potassium peroxymonosulfate (PMS, HSO$_5^-$), potassium

persulfate (PS, $K_2S_2O_8$), and the quenching agent sodium thiosulfate ($Na_2S_2O_3$) were used.

2.4.1. PAHs Measurements

For PAHs and some metabolites (hydroxy-benzoic acid, benzoic acid) analyses the samples were first filtered through a glass fiber filter (47 mm-diameter) and to collect the particle-phase in series with a resin column (~10 g XAD-2) and to collect dissolved-phase polybrominated diphenyl ethers. Resin and water filters were ultrasonically extracted for 60 min with a mixture of 1/1 acetone: hexane. All extracts were analyzed for four PAHs (Table 1) gas chromatographically (Agilent 6890N GC) equipped with a mass selective detector (Agilent 5973 inert MSD). A capillary column (HP5-MS, 30 m, 0.25 mm, 0.25 µm) was used. The initial oven temperature was kept at 50°C for 1 min, then raised to 200°C at 25°C/min and from 200°C to 300°C at 8°C/min, and then maintained for 5.5 min. High purity He(g) was used as the carrier gas at constant flow mode (1.5 ml/min, 45 cm/s linear velocity). PAHs and their metabolites were identified on the basis of their retention times, target and qualifier ions and were quantified using the internal standard calibration procedure. To determine the degradation intermediates, samples (10 ml each) were collected at 0 min, 30 min, 120 min, 240 min and 360 min. The hydrophobic PAHs (ACL, CRB, BaP and BkF) were performed using a HPLC (Agilent-1100) with a method developed by Lindsey and Tarr, [51]. The chromatographic conditions for the hydrophobic PAHs (ACL, CRB, BaP and BkF) determination were as follows: C-18 reverse phase HPLC column (Ace 5C18; 25-cm x 4.6-mm, 5 µm, mobile phase: 50/50 (v/v) methanol/organic-free reagent water). pH, temperature, oxidation-reduction potential (ORP) were monitored following Standard Methods 2550, 2580 and 5220 D, [52]. H_2O_2 was quantified with a colorimetric method following Standard Method 3550, [52].

Table 1: Energy efficiency of photocatalysis with different sun light intensities at ambient conditions after 360 min sun light irradiation time in petrochemical industry wastewater (n=3, mean values, n: deionized water and petrochemical industry wastewater containing PAHs)

Energy efficiency of photocatalysis with different sun light intensities			
Sun light intensity (W/cm^2)	Power density (W/ml)	Specific energy (kWh/kg COD-in influent)	COD removal efficiency (%)
17	0.12	8.29	47
38	0.91	8.90	59
24.03	1.34	9.26	68
39.09	1.71	9.91	77
46	1.97	10.83	80
52.3	2.38	12.42	86

2.5. Data Analysis

The pseudo-first-order kinetic model was employed to fit the kinetic data, [12, 50], (Equation 1):

$$\ln\left(\frac{C_t}{C_0}\right) = -k \cdot t \qquad (1)$$

Where, C_t and C_0 are the PAHs concentrations (µg/l) at the reaction time of t and 0 min, respectively, and k is the rate constant (1/min). The integration of UV–Vis absorbance of PAHs was achieved using the software OriginPro 8 (OriginLab Corporation, Northampton, MA, USA). The correlation fittings between the reaction rate constant and various water quality parameters were conducted by using OriginPro 8 or GraphPad Prism 6 (GraphPad Software, Inc., La Jolla, CA, USA). The fitting models included fourth-order polynomial and sigmoidal (Boltzmann and DoseResp functions) equations.

2.6. *Daphnia magna* Acute Toxicity Test

To test toxicity 24 h old *Daphnia magna* were used as described in Standard Methods, [52]. After preparing the test solution, experiments were carried out using 5 or 10 *Daphnia magna* introduced into the test vessels. These vessels had 100 ml of effective volume at pH=7.0-8.0, providing a minimum DO concentration of 6 mg/l at an ambient temperature of 20°C-25°C. Young *Daphnia magna* were used in the test (≤ 24 h old). A 24 h exposure is generally accepted as standard for a *Daphnia* acute toxicity test. The results were expressed as mortality percentage of the *Daphnia magna*. Immobile animals were reported as dead *Daphnia magna*.

2.7. Statistical Analysis

ANOVA analysis of variance between experimental data was performed to detect F and P values, i.e. the ANOVA test was used to test the differences between dependent and independent groups, [53]. Comparison between the actual variation of the experimental data averages and standard deviation is expressed in terms of F ratio. F is equal (found variation of the date averages/expected variation of the date averages). P reports the significance level, d.f indicates the number of degrees of freedom. Regression analysis was applied to the experimental data in order to determine the regression coefficient R^2 (Statgraphics, Centurion XV, sofware, 2005), [54]. The aforementioned test was performed using Microsoft Excel Program.

All experiments were carried out three times and the results are given as the means of triplicate samplings. The data relevant to the individual pollutant parameters are given as the mean with standard deviation (SD) values.

3. Results and Discussion

3.1. Raw Wastewater

Characterization of raw petrochemical wastewater taken from the influent of the aeration unit of a petrochemical industry wastewater treatment plant, İzmir, Turkey was performed. The results are given as the mean value of triplicate sampling. The mean values for pH, ORP were recorded as 7.21 mV and 28.20 mV, respectively. The mean TSS and TVSS concentrations were measured as 310.3 mg/l and 250.6 mg/l, respectively. The mean DO, BOD_5, COD_{total}, $COD_{dissolved}$ concentrations were 1.78 mg/l, 584 mg/l, 1475 mg/l and 1127 mg/l while the Total-N, NH_4-N, NO_3-N, NO_2-N, Total-P, PO_4-P and oil concentrations were measured as 15.40 mg/l, 2.20 mg/l, 1.80 mg/l, 0.05 mg/l, 10.60 mg/l, 6.80 mg/l and 206 mg/l, respectively. The less hydrophobic ACL and CRB concentrations were 124.2 mg/l and 3.60 mg/l while the more hydrophobic BaP and BkF concentrations were measured as 5.41 mg/l and 0.64 mg/l, respectively, in the petrochemical industry wastewater. Physical and chemical properties of the PAHs in petrochemical industry wastewater studied in this work was shown at Table 2.

* Table 2 can be found in Appendix section.

3.2. Characterization of photocatalysts

The XRD spectra of the prepared nanocomposites (GO-Sr(OH)₂/SrCO₃ and GO-TiO₂-Sr(OH)₂/SrCO₃) (Figure 1). For both composite materials, the diffraction peak at about 2θ=10° is attributed to GO, [55]. For GO-Sr(OH)₂/SrCO₃, the broad peaks at 2θ=25°, 2θ=28°, 2θ=36° and 2θ=43° are assigned to the crystalline phase of SrCO₃ (JCPDS Card No. 005-0418), whereas weak peaks for Sr(OH)₂, Sr(OH)₂.H₂O and Sr (OH)₂.8H₂O were also observed as confirmed by JCPDS Cards Nos. 27-0847, 28-1222, and 27-1438, respectively, [56]. The XRD pattern of GOTiO₂-Sr(OH)₂/SrCO₃ showed much sharper peaks than those of GO-Sr (OH)₂/SrCO₃, indicating well-developed crystalline phases. The peaks at 2θ=25°, 2θ=28°, 2θ=36° and 2θ=43° are attributed to TiO₂ belonging to the rutile phase (JCPDS Card No. 88-1175), while minor peaks from the anatase phase (JCPDS Card No. 84-1268) were also observed, [49, 57]. Besides, the peaks at 2θ=24°, 2θ=32.7°, 2θ=40.1°, 2θ=46.6°, 2θ=57.8° and 2θ=67.9° can be attributed to the perovskite-type phase of cubic symmetry of SrTiO₃ (STO) (JCPDS Card No. 86-0179), [58, 59].

* Figure 1 can be found in Appendix section.

The SEM images with the EDX maps of the elemental distribution (Figure 2a, Figure 2b, Figure 2c, Figure 2d, Figure 2e), Sr and/or Ti's GO-Sr(OH)₂/SrCO₃ and GO-TiO₂-Sr(OH)₂/SrCO₃ reveals that it is distributed quite uniformly in nanocomposite matrices. The nano-rods in Figure (2a) are SrCO₃, while the nanospheres on the GO surface in Figure (2c) are likely to be the aggregates of SrTiO₃ nanoparticles with an average diameter of about 1 μm, [60].

* Figure 2 can be found in Appendix section.

Figure (3a) shows the FTIR spectrum for GO. The characteristic bands are assigned as follows: carboxyl groups at 1070 1/cm and 1760 1/cm, C]C stretching vibration of the sp2 carbon skeletal network at 1600 1/cm, OH groups at 1380 1/cm and 1000 1/cm , and epoxy groups at 900 1/cm, [55]. The peak at 1240 1/cm can be attributed to the S]O asymmetric stretching vibrations arising from sulfones or sulfates that were formed upon graphite oxidation with H_2SO_4 (SI Text S1). Figure (3b) presents the FTIR spectra of the nanocomposite materials, i.e., GO-Sr (OH)₂/SrCO₃ and GO-TiO₂-Sr(OH)₂/SrCO₃. The characteristic bands of GO are clearly seen in the spectra of both nanocomposites. For GO-Sr (OH)₂/SrCO₃, the bands at 1071 1/cm and 1760 1/cm are attributed to the asymmetric and symmetric stretching vibrations of the carboxylate groups. The band at 1446 1/cm is attributed to the asymmetric stretching vibration of carbonate anion

(CO_3^{-2}) in $SrCO_3$ that has a D3h symmetry, while the bands at 860 1/cm and 600 1/cm are assigned to the vibrations of the CO_3^{-2} due to bending out of plane and in plane, respectively, [56]. The bands at 3200 1/cm, 1380 1/cm and 1000 1/cm are due to stretching mode of –OH groups and can be attributed to $Sr(OH)_2$, $Sr(OH)_2.H_2O$ and $Sr(OH)_2.8H_2O$. For $GO-TiO_2-Sr(OH)_2/SrCO_3$, a new broad peak was observed in the range of 550–780 1/cm, which can be ascribed to the TiO_2 stretching, [60]. The bands at 1760 1/cm and 1384 1/cm for the carboxylate groups disappeared, indicating that these groups have been bounded to TiO_2. The bands at 3200 1/cm, 1384 1/cm and 1020 1/cm were diminished, indicating that less crystalline phases of $Sr(OH)_2$, $Sr(OH)_2.H_2O$ and/or $Sr(OH)_2.8H_2O$ were formed, [56].

* Figure 3 can be found in Appendix section.

The textural features of the nanocomposites were investigated with the N_2 adsorption-desorption isotherms and the results are shown in Figure 4a. According to the International Union of Pure and Applied Chemistry (IUPAC), the shape of the isotherm for the $GO-Sr(OH)_2/SrCO_3$ nanocomposite can be classified as a combination of Type II and Type III, indicating the coexistence of mesopores and macropores, [61]. The deviation of the desorption isotherm from the adsorption isotherm (hysteresis) can be attributed to the presence of slit or bottle neck pores. The isotherm displayed a significant increase of N_2 uptake at $P/P_o > 0.95$, indicating the presence of external surface area and/or textural porosity. In contrast, the isotherm for $GO-TiO_2-Sr(OH)_2/SrCO_3$ conforms to the Type II isotherm, which is characteristic of low-porosity materials or materials with large macropores, [61]. The decrease of the mesopores and macropores volume in $GO-TiO_2-Sr(OH)_2/SrCO_3$ can be attributed to occupying part of the pores by TiO_2 and $SrTiO_3$ reaction products. The inset in Figure 4b presents the pore size distributions for GO, $GO-Sr(OH)_2/SrCO_3$ and $GO-TiO_2-Sr(OH)_2/SrCO_3$ estimated by the density functional theory (DFT) calculations of the N_2 adsorption data. The presence of mesopores and macropores is clearly evident in GO, which are then sharply diminished with the addition of $Sr(OH)_2/SrCO_3$ and TiO_2. Moreover, the specific surface area of $GO-TiO_2-Sr(OH)_2/SrCO_3$ (5.64 m^2/g) was found 75% less than that of $GO-Sr(OH)_2/SrCO_3$ (21.47 m^2/g), and the pore volume of $GO-TiO_2-Sr(OH)_2/SrCO_3$ (0.0319 cm^3/g) was 84% less than that of $GO-Sr(OH)_2/SrCO_3$ (0.1842 cm^3/g).

* Figure 4 can be found in Appendix section.

3.3. Effect of Increasing GO Nanoparticle Concentrations during Hydrophobic PAHs Treatment with Photocatalytic Degradation under Sun Light Irradiation

Preliminary studies showed that the optimum sun light intensity, irradiation time, pH, and temperature were 100 mW/cm^2, 360 min, pH=7.0 and at 22°C, respectively in the presence of 7 mg/l GO nanocomposite concentration (data not shown). The effects of increasing GO nanoparticle concentrations (2 mg/l, 4 mg/l and 8 mg/l) on the removals of PAHs [less hydrophobic (ACL, CRB) and more hydrophobic (BaP, BkF)] in petrochemical industry wastewater under 100 mW/cm^2 sun light intensity, at 360 min sun light irradiation time, at pH=7.0 and at 22°C, respectively (Table 3; SET 1). The maximum removals of 87%ACL, 87%CRB, 85%BaP and 84%BkF hydrophobic PAHs in petrochemical industry wastewater were measured at 8 mg/l GO nanoparticle concentration under 100 mW/cm^2 sun light intensity, at 100 W photocatalytic power, at 360 min sun light irradiation time, at pH=7.0 and at 22°C, respectively (Table 3; SET 1). The increasing GO nanoparticle concentrations were positively affect the photocatalytic degradation of hydrophobic PAHs (ACL, CRB, BaP and BkF) (Table 3; SET 1).

* Table 3 can be found in Appendix section.

3.4. Effect of Increasing TiO₂ Nanoparticle Concentrations during Hydrophobic PAHs Treatment with Photocatalytic Degradation under Sun Light Irradiation

The preliminary studies showed that the optimum removals for PAHs [less hydrophobic (ACL, CRB) and more hydrophobic (BaP, BkF)] were obtained at 8 mg/l TiO_2 concentration, under 98 mW/cm^2 sun light intensity, at 95 W photocatalytic power, at 350 min sun light irradiation time, at pH=7.1 and at 22°C (data not shown). The effects of increasing TiO_2 nanoparticle concentrations (1 mg/l, 3 mg/l, 6 mg/l and 9 mg/l) were measured to detect the PAHs yields [less hydrophobic (ACL, CRB) and more hydrophobic (BaP, BkF)] in petrochemical industry wastewater under 100 mW/cm^2 sun light intensity, at 100 W photocatalytic power, at 360 min sun light irradiation time, at pH=7.0 and at 22°C, respectively (Table 3; SET 2). The removals of BaP, BkF, ACL and CRB PAHs increased from 75% up to 86% as the TiO_2 nanoparticle concentrations was increased

from 1 mg/l up to 6 mg/l, whereas 1 mg/l - 3 mg/l TiO_2 nanoparticle concentrations did not significantly contribute to the hydrophobic PAHs (ACL, CRB, BaP and BkF) removals in petrochemical industry wastewater (Table 3; SET 2). The maximum 89%ACL, 90%CRB, 91%BaP and 92%BkF hydrophobic PAHs removals in petrochemical industry wastewater were detected at 9 mg/l TiO_2 nanoparticle concentration, under 100 mW/cm^2 sun light intensity, at 100 W photocatalytic power, at 360 min sun light irradiation time, at pH=7.0 and at 22°C, respectively (Table 3; SET 2). The increasing of TiO_2 nanoparticle concentrations positively affected the photocatalytic degradation of hydrophobic PAHs (ACL, CRB, BaP and BkF) in petrochemical industry wastewater during sun light irradiation process (Table 3; SET 2).

3.5. Effect of Increasing GO-TiO_2-Sr(OH)$_2$/SrCO$_3$ Nanocomposite Concentrations during Hydrophobic PAHs Treatment with Photocatalytic Degradation under Sun Light Irradiation

Based on the preliminary studies the optimum removals of some less hydrophobic (ACL, CRB) and more hydrophobic (BaP, BkF)] PAHs in petrochemical industry wastewater were researched at 100 mW/cm^2 sun light intensity, at 100 W photocatalytic power, at 360 min sun light irradiation time, at pH=7.0 and at 22°C, respectively at 3 mg/l GO-TiO_2-Sr(OH)$_2$/SrCO$_3$ concentrations (Table 3; SET 3). The removals in BaP, BkF, ACL and CRB in petrochemical industry wastewater increased from 92%, up to 99% as the GO-TiO_2-Sr(OH)$_2$/SrCO$_3$ nanocomposite concentration was increased from 1 up to 4 mg/l, at 100 mW/cm^2 sun light intensity, at 100 W photocatalytic power, at 360 min sun light irradiation time and at 22°C, respectively (Table 3; SET 3). The maximum 97%ACL, 98%CRB, 98%BaP and 99%BkF hydrophobic PAHs removals in petrochemical industry wastewater were found at 4 mg/l GO-TiO_2-Sr(OH)$_2$/SrCO$_3$ nanocomposite concentration under 100 mW/cm^2 sun light intensity, at 100 W photocatalytic power, at 360 min sun light irradiation time, at pH=7.0 and at 22°C, respectively. The increasing GO-TiO_2-Sr(OH)$_2$/SrCO$_3$ nanocomposite concentrations were found to be positively affect for the photocatalytic degradation of hydrophobic PAHs (ACL, CRB, BaP and BkF) in petrochemical industry wastewater (Table 3; SET 3).

An optimum GO-TiO_2-Sr(OH)$_2$/SrCO$_3$ nanocomposite concentration of 4 mg/l increase the

ionic strength of the aqueous phase, driving the PAHs to the bulk–bubble interface in a photocatalytic reactor. This, increases the partitioning of the PAH species upon radical scavengers in a photocatalytic reactor. Beyond the partitioning enhancement, the presence of salt reduces the vapor pressure and increases the surface tension of the PAHs, [62]. Therefore, the solubility of the solution decreases and the diffusion of solutes decreases from the bulk solution to the bubble–liquid interface with administration of decreasing GO-TiO_2-Sr(OH)$_2$/SrCO$_3$ nanocomposite concentrations in the photocatalytic reactor, [63]. The high PAH removals in raised GO-TiO_2-Sr(OH)$_2$/SrCO$_3$ nanocomposite concentrations can be explained by the fact that a higher amount of GO-TiO_2-Sr(OH)$_2$/SrCO$_3$ nanocomposite will create more salting out effect than the lower amount and thus increase the interfacial concentration of the PAHs. In our study, no contribution of GO-TiO_2-Sr(OH)$_2$/SrCO$_3$ nanocomposite > 4 mg/l to the PAH yields could be attributed to the synergistic and antagonistic effects of the by-products and to the more hydrophobic (BaP, BkF) and less hydrophobic (ACL, CRB) nature of PAHs present in petrochemical industry wastewaters (Table 3; SET 3).

3.6. Effect of Increasing Sun Light Irradiation Times during Hydrophobic PAHs Treatment with Photocatalytic Degradation under Sun light Irradiation

The effects of increasing sun light irradiation times (30 min, 120 min, 240 min and 360 min) were measured in PAHs [less hydrophobic (ACL, CRB) and more hydrophobic (BaP, BkF)] in petrochemical industry wastewater under 100 mW/cm^2 sun light intensity, at 100 W photocatalytic power, at pH=7.0 and at 22°C, respectively (Table 3; SET 4).

The removals of BaP, BkF, ACL and CRB increased from 56%-65% up to 72%-79% as the sun light irradiation times was increase from 30 min up to 240 min, whereas 30 min - 120 min sun light irradiation times dis not significantly contribute to the hydrophobic PAHs (ACL, CRB, BaP and BkF) removals in petrochemical industry wastewater was not observed (Table 3; SET 4). The maximum 81%ACL, 80%CRB, 80%BaP and 84%BkF hydrophobic PAHs removals in petrochemical industry wastewater were indicated at 360 min sun light irradiation time, under 100 mW/cm^2 sun light intensity, at 100 W photocatalytic power, at pH=7.0 and at 22°C, respectively (Table 3; SET 4). The

increasing sun light irradiation times were affected positively effect for the photocatalytic degradation hydrophobic PAHs (ACL, CRB, BaP and BkF) in petrochemical industry wastewater during sun light irradiation process (Table 3; SET 4).

3.7. Effect of Increasing Photocatalytic Powers during Hydrophobic PAHs Treatment with Photocatalytic Degradation under Sun Light Irradiation

The effects of increasing photocatalytic powers (10 W, 50 W and 100 W) were measured in PAHs [less hydrophobic (ACL, CRB) and more hydrophobic (BaP, BkF)] in petrochemical industry wastewater under 100 mW/cm^2 sun light intensity, at 360 min sun light irradiation time, at pH=7.0 and at 22°C, respectively (Table 3; SET 5).

The removals of BaP, BkF, ACL and CRB increased from 56%-69% up to 69%-78% as the photocatalytic powers was increase from 10 W up to 50 W, whereas 10W-50 W photocatalytic powers did not significantly contribute to the hydrophobic PAHs (ACL, CRB, BaP and BkF) removals in petrochemical industry wastewater was not obtained (Table 3; SET 5). The maximum 84%ACL, 86%CRB, 88%BaP and 89%BkF hydrophobic PAHs removals in petrochemical industry wastewater were indicated at 100 W photocatalytic power, under 100 mW/cm^2 sun light intensity, at 360 min sun light irradiation time, at pH=7.0 and at 22°C, respectively (Table 3; SET 5). The increasing photocatalytic powers were affected positively effect for the photocatalytic degradation hydrophobic PAHs (ACL, CRB, BaP and BkF) in petrochemical industry wastewater during sun light irradiation process (Table 3; SET 5).

3.8. Photocatalytic Activity

PAHs is resistant to photolysis under sun light, [63]. The control tests showed that nearly 85% of PAHs in petrochemical industry wastewater still retained in the solution after 360 min sun irradiation time (Table 4 and Figure 5) and the pseudo-first-order rate constant was k=0.0006±0.0001 1/min. The addition of TiO$_2$ nanoparticle in petrochemical industry wastewater enhanced the photodegradation rate by 3 folds (k=0.0016 1/min) (Table 4 and Figure 5). The addition of GO in petrochemical industry wastewater increased the photodegradation yield (k=0.0019±0.0001 l/min) (Table 4 and Figure 5). The UV light in the sun light irradiation is the main driving energy for the photocatalytic activity of TiO$_2$, [12]. The synthesized GO-Sr(OH)$_2$/SrCO$_3$ showed a slightly better photocatalytic activity

(k=0.0021±0.0001 1/min) than TiO$_2$ and GO nanoparticle in petrochemical industry wastewater (Table 4 and Figure 5). As expected, the GO-TiO$_2$-Sr(OH)$_2$/SrCO$_3$ nanocomposite in petrochemical industry wastewater exhibited the highest photocatalytic activity and greatly accelerated the photocatalytic degradation rate. It was shown a synergistic interaction among the three nanocomponents, i.e., GO, TiO$_2$ and Sr(OH)$_2$/SrCO$_3$, which can facilitate utilization of both UV and visible light energy in the sun light irradiation in petrochemical industry wastewater.

Table 4: The rate constants of GO, TiO$_2$ and GO-TiO$_2$-Sr(OH)$_2$/SrCO$_3$ after photocatalytic degradation with sun light irradiation process in petrochemical industry wastewater.

Sun light irradiation time (min)	k (1/min)			
	Control	GO	TiO$_2$	GO-TiO$_2$-Sr(OH)$_2$/SrCO$_3$
30	0.0001± 0.00001	0.0005± 0.0001	0.0004± 0.0001	0.0009±0.0001
120	0.0003± 0.0001	0.0011± 0.0001	0.0009± 0.0001	0.0013±0.0001
240	0.0005± 0.0001	0.0014± 0.0001	0.0012± 0.0001	0.0017±0.0001
360	0.0006± 0.0001	0.0019± 0.0001	0.0016± 0.0001	0.0021±0.0001

* Figure 5 can be found in Appendix section.
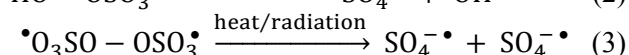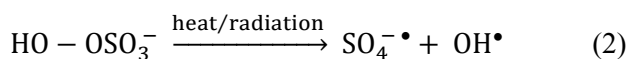
In the photocatalytic activity of GO-TiO$_2$-Sr(OH)$_2$/SrCO$_3$ firstly, the hybridization of the two coupling semiconductors (TiO$_2$ and Sr(OH)$_2$/SrCO$_3$) shifted the optical absorption to the higher wavelength region and impel the transfer of photo-excited electron and holes to opposite directions (data not shown), [16, 21, 64]. Secondly, the GO sheets can further promote the transport of the photo-excited electrons, and thus inhibit the recombination of electrons and holes. And thirdly, the reaction product SrTiO$_3$ has high photocatalytic activity, [64], and can also contribute to the enhanced photodegradation of PAHs.

3.9. Contribution of Reactive Oxygen Species (ROS) on the Photocatalytic Yields of PAHs
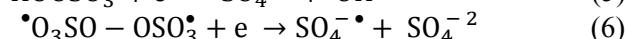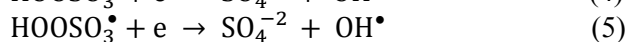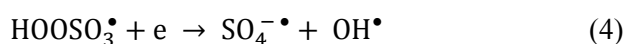
In generally, photocatalytic oxidation processes, ROS (potassium peroxymonosulfate (PMS, HSO$_5^-$), potassium persulfate (PS, K$_2$S$_2$O$_8$) and the

quenching agent sodium thiosulfate ($Na_2S_2O_3$) generated during the photocatalytic reactions are mainly responsible for the degradation of organic pollutants, [65]. Preliminary studies showed that among the concentrations studied with 1.1 mg/l PMS, 0.9 mg/l PS and 0.79 mg/l $Na_2S_2O_3$ highest photooxidation yields was detected.
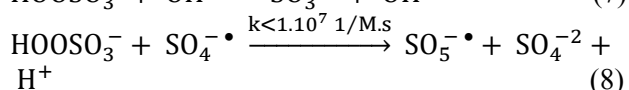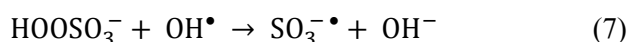
PS and PMS can undergo homolytic dissociation of the peroxide bond from radiation or thermal activation and give SO_4^- • radicals, and SO_4^- and $OH^•$ radicals, respectively (Equation 2 and Equation 3), [41].

$$HO - OSO_3^- \xrightarrow{\text{heat/radiation}} SO_4^{-•} + OH^• \qquad (2)$$
$$^•O_3SO - OSO_3^• \xrightarrow{\text{heat/radiation}} SO_4^{-•} + SO_4^{-•} \qquad (3)$$

The oxidants can also act as electron acceptors of the photo-excited electron from the conduction band of $GO-TiO_2-Sr(OH)_2/SrCO_3$ and through electron transfer mechanisms to give additional SO_4^- • radical and $OH^•$ radical based on the reactions listed below (Equation 4, Equation 5 and Equation 6), [66- 68].

$$HOOSO_3^• + e \rightarrow SO_4^{-•} + OH^• \qquad (4)$$
$$HOOSO_3^• + e \rightarrow SO_4^{-2} + OH^• \qquad (5)$$
$$^•O_3SO - OSO_3^• + e \rightarrow SO_4^{-•} + SO_4^{-2} \qquad (6)$$

Heat activation of oxidants did not contribute on radical formation because of the temperature in the reactor and the relatively short treatment times compared to what was reported needed in the literature, [41]. On the other hand, homolytic dissociation of the peroxide bond of the oxidants through radiation seems to be a more probable mechanism. Even though, both oxidants have low absorption in the UVA range, the adsorption of PS at λ=365 nm is four times the one of PMS, when measured in solutions of the same concentration of active species, [39]. This indicates that PS has a better ability to adsorb photons compared to PMS and therefore, more radicals can be formed. The remaining PMS and form peroxymonosulfate radicals (SO_5^- •) (Equation 7 and Equation 8) that have significantly reduced oxidation ability and higher selectivity (redox potential 1.1 V, at pH=7.0) to SO_4^- • radicals (Table 5).

$$HOOSO_3^- + OH^• \rightarrow SO_3^{-•} + OH^- \qquad (7)$$
$$HOOSO_3^- + SO_4^{-•} \xrightarrow{k<1.10^7 \text{ 1/M.s}} SO_5^{-•} + SO_4^{-2} + H^+ \qquad (8)$$

On the other hand, reaction of PS with a SO_4^- • radical will cause the formation of another SO_4^- •

radical (Equation 9) which leaves the oxidative capacity of the system unaltered. The effects of (PMS, HSO_5^-), (PS, $K_2S_2O_8$) and $Na_2S_2O_3$ on the photocatalytic degradation rates of the studied BkF PAH were tabulated (Table 5).

$$^•O_3SO - OSO_3^• + SO_4^{-•} \rightarrow SO_4^{-•} + 2SO_4^{-2} \qquad (9)$$
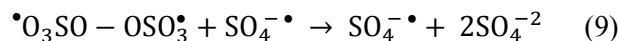
Table 5: Contributions of ROS to photocatalytic degradation of BkF PAH in petrochemical industry wastewater by $GO-TiO_2-Sr$ $(OH)_2/SrCO_3$ under simulated solar irradiation.

Scavengers	Scavenging radicals	k (1/min)
None (Only $GO-TiO_2-Sr$ $(OH)_2/SrCO_3$)	-	0.0061
PMS	HSO_5^-	0.0062
PS	$K_2S_2O_8$	0.0067
$Na_2S_2O_3$	SO_4^{-2}	0.0063

3.10. Photodegradation Pathway

At Table 6 and Figure 6 presents the reaction intermediates during the photocatalytic degradation of hydrophobic PAHs (ACL, CRB, BaP and BkF) in petrochemical industry wastewater by $GO-TiO_2-Sr(OH)_2/SrCO_3$ under sun light irradiation process. It is noteworthy that the reaction rate and selectivity can be altered by the reaction matrix. For example, using dimethyl carbonate instead of water as the medium, the selectivity of TiO_2 for the partial photooxidation of hydrophobic PAHs (ACL, CRB, BaP and BkF) in petrochemical industry wastewater was enhanced.

Table 6: By-products of BkF, BaP and ACL PAHs in petrochemical industry wastewater at 100 mW/cm^2 sun light intensity, at 250 ml solution volume, at 1 mg/l initial PAHs concentration, at pH=7.0±0.2, at 22°C, at 360 min sun light irradiation time, respectively (n=3, mean±SD).

PAHs name	Initial PAH concentration (mg/l)	Photocatalytic degradation metabolites (mg/l)
BkF	0.804 ± 0.001	benzoic acid: 0.21 ± 0.002 FL: 0.59 ± 0.005
BaP	0.077 ± 0.003	benzoic acid: 0.028 ± 0.001 PY: 0.0040 ± 0.00014
ACL	53.42 ± 0.05	NAP: 44.13 ± 0.07

* Figure 6 can be found in Appendix section.

3.11. Determination of the Acute Toxicity of Studied PAHs on *Daphnia magna* before and after Treatment of Hydrophobic PAHs under Photocatalytic Degradation at Different Experimental Conditions

The raw petrochemical industry wastewater samples induced 95% motility inhibition to *Daphnia magna* cells (Table 7). This inhibition could be attributed to the mixed recalcitrant carcinogenic hydrophobic PAHs with high benzene rings and to the synergistic effects of the aforementioned more hydrophobic PAHs with less hydrophobic PAHs in petrochemical industry wastewaters. When *Daphnia magna* were exposed to the effluent samples treated with only photolysis without catalyst at 22°C for 360 min sun light irradiation time a significant reduction in inhibition (10.01%) was not observed (the inhibition decreased from initial 98% to 88%). In other words, photolysis alone was not sufficient to remove the toxicity of recalcitrant by-products from the petrochemical industry wastewater (Table 7). The maximum removals in inhibition were observed in photocatalytic degraded petrochemical industry wastewater containing 8 mg/l GO nanoparticle, 9 mg/l TiO_2 nanoparticle and 4 mg/l GO-TiO_2-Sr(OH)$_2$/SrCO$_3$ nanocomposite concentrations at a neutral pH=7.0 after 360 min sun light irradiation time, at 22°C, respectively. A decreasing toxicity trend due to long sun light irradiation time with catalyst can be explained by the formation of less toxic by-products over time. The petrochemical industry wastewater containing TiO_2 nanoparticles > 10 mg/l displayed toxicity to *Daphnia magna* after 360 min sun light irradiation time. Similarly, GO

nanoparticle and GO-TiO_2-Sr(OH)$_2$/SrCO$_3$ nanocomposite concentrations > 10 mg/l and > 6 mg/l caused inhibition to *Daphnia magna* motility after 360 min sun light irradiation time and at 22°C. A significant correlation between *Daphnia manga* acute toxicity and TiO_2, GO and GO-TiO_2-Sr(OH)$_2$/SrCO$_3$ nanocomposite concentrations in petrochemical industry wastewater was observed after 360 min sun light irradiation time according to multiple regression analysis (R^2=0.87, F=17.99. p=0.001).

* Table 7 can be found in Appendix section.

Toxicity results showed that both high concentrations of GO, TiO_2 and GO-TiO_2-Sr(OH)$_2$/SrCO$_3$ influence the toxicity of PAH mixtures which may interact with the PAHs and their degraded metabolites to form different by-products during photocatalytic degradation in petrochemical industry wastewater. These by-products exhibit synergistic and antagonistic toxicity effects on *Daphnia magna* as well. The effective PAH concentrations in petrochemical industry wastewater caused 50% mortality in *Daphnia magna* cells (EC_{50} value as mg/l) increased from initial 342.56 mg/l to EC_{50}=631.05 mg/l, at pH=7.0 and at 22°C after 360 min sun light irradiation time resulting in a maximum acute toxicity removal of 99.99% at 1 mg/l GO-TiO_2-Sr(OH)$_2$/SrCO$_3$ nanocomposite concentration (Table 7; SET 1). The EC_{50} value increased from initial 342.56 mg/l to EC_{50}=587.45 mg/l at 6 mg/l TiO_2 concentration in petrochemical industry wastewater after 360 min sun light irradiation time, at pH=7.0 and at 22°C resulting in a maximum acute toxicity removal of 94% (Table 7; SET 3). The EC_{50} value increased from initial 342.56 mg/l to EC_{50}=630.45 mg/l at 8 mg/l GO nanoparticle concentration in petrochemical industry wastewater was measured to 99.94% maximum acute toxicity removal, at pH=7.0, at 22°C after 360 min sun light irradiation time, respectively (Table 7; SET 3). In this acute toxicity reduction, the EC_{50} value of petrochemical industry wastewater increased to EC_{50}=631.05 mg/l. Low acute toxicity removals found at high GO nanoparticle concentrations in petrochemical industry wastewater could be attributed to their detrimental effect on the *Daphnia magna* cells (Table 7; SET 1).

A strong significant correlation between EC_{50} values and PAH removals showed that the *Daphnia magna* acute toxicity test alone can be considered aa a reliable indicator of petrochemical industry wastewater toxicity (R^2=0.87, F=17.99. p=0.001).

Similarly, a strong linear correlation between threshold concentrations of GO, TiO_2, GO-TiO_2-$Sr(OH)_2$/$SrCO_3$ and decrease in inhibitions in petrochemical industry wastewater was observed ($R^2 = 0.91$, F=3.89, p=0.001) while the correlation between the inhibition decrease and GO, TiO_2 and GO-TiO_2-$Sr(OH)_2$/$SrCO_3$ nanocomposite concentrations above the threshold values was weak and not significant ($R^2 = 0.38$, F=3.81, p=0.001). In this study, the *Daphnia magna* acute toxicity test alone can be considered a reliable indicator of petrochemical industry wastewater toxicity.

4. Conclusions

The results of this study showed that the hydrophobic PAHs in a real petrochemical industry wastewater with high benzene rings could be removed as successfully as the less hydrophobic PAHs (ACL and CRB) and more hydrophobic PAHs (BaP and BkF) with photocatalytic degradation under sun light irradiation process.

The maximum removals of 87%ACL, 87%CRB, 85%BaP and 84%BkF hydrophobic PAHs in petrochemical industry wastewater were observed at 8 mg/l GO nanoparticle concentration under 100 mW/cm^2 sun light intensity, at 100 W photocatalytic power, at 360 min sun light irradiation time, at pH=7.0 and at 22°C, respectively. The maximum 89%ACL, 90%CRB, 91%BaP and 92%BkF hydrophobic PAHs removals in petrochemical industry wastewater were detected at 9 mg/l TiO_2 nanoparticle concentration, under 100 mW/cm^2 sun light intensity, at 100 W photocatalytic power, at 360 min sun light irradiation time, at a pH of 7.0 and at 22°C, respectively. The maximum 97%ACL, 98%CRB, 98%BaP and 99%BkF hydrophobic PAHs removals in petrochemical industry wastewater were found at 4 mg/l GO-TiO_2-$Sr(OH)_2$/$SrCO_3$ nanocomposite concentration under 100 mW/cm^2 sun light intensity, at 100 W photocatalytic power, at 360 min sun light irradiation time, at pH=7.0 and at 22°C, respectively.

The addition of TiO_2 nanoparticle in petrochemical industry wastewater enhanced the photodegradation rate by 3 folds (k=0.0016 1/min). The addition of GO nanoparticle in petrochemical industry wastewater increased the photodegradation yield (k=0.0019±0.0001 l/min). The synthesized GO-$Sr(OH)_2$/$SrCO_3$ in petrochemical industry wastewater showed a slightly better photocatalytic activity (k=0.0021±0.0001 1/min) than TiO_2 and GO nanoparticle. As expected, the GO-TiO_2-$Sr(OH)_2$/$SrCO_3$ nanocomposite in petrochemical industry wastewater exhibited the highest photocatalytic activity and greatly accelerated the photocatalytic degradation rate. It was shown a synergistic interaction among the three nanocomponents, i.e., GO, TiO_2 and $Sr(OH)_2$/$SrCO_3$, which can facilitate utilization of both UV and visible light energy in the sun light irradiation. 1.1 mg/l PMS, 0.9 mg/l PS and 0.79 mg/l $Na_2S_2O_3$ highest photooxidation yields in petrochemical industry wastewater was detected.

The effective PAH concentrations in petrochemical industry wastewater caused 50% mortality in *Daphnia magna* cells (EC_{50} value as mg/l) increased from initial 342.56 mg/l to EC_{50}=631.05 mg/l, at pH=7.0 and at 22°C after 360 min sun light irradiation time resulting in a maximum acute toxicity removal of 99.99% at 1 mg/l GO-TiO_2-$Sr(OH)_2$/$SrCO_3$ nanocomposite concentration.

In sum, GO-TiO_2-$Sr(OH)_2$/$SrCO_3$ nanocomposites in petrochemical industry wastewater holds the potential to serve as a highly effective and robust photocatalyst for energy-effective photodegradation of PAHs (and potentially other persistent organic pollutants) in complex water matrices, and the multiplicative model is a useful tool for predicting the photocatalytic performances under several experimental conditions.

Acknowledgement:

References:
[1] J. Fu, S. Sheng, T. Wen, Z.-M. Zhang, Q. Wang, Q.-X. Hu, Q.-S. Li, S.-Q. An, H.-L. Zhu, Polycyclic aromatic hydrocarbons in surface sediments of the Jialu River, *Ecotoxicology,* Vol.20, 2011a, pp. 940–950.

[2] J. Fu, Y. Gong, X. Zhao, S.E. O'Reilly, D. Zhao, Effects of oil and dispersant on formation of marine oil snow and transport of oil hydrocarbons, *Environmental Science & Technology,* Vol.48, 2014, pp. 14392–14399.

[3] Y. Gong, J. Fu, S.E. O'Reilly, D. Zhao, Effects of oil dispersants on photodegradation of pyrene in marine water, *Journal of Hazardous Materials,* Vol.287, 2015, pp. 142–150.

[4]   J. Fu, Y.-H. Ding, L. Li, S. Sheng, T. Wen, L.-J. Yu, W. Chen, S.-Q. An, H.-L. Zhu, Polycyclic aromatic hydrocarbons and ecotoxicological characterization of sediments from the Huaihe River, China, *Journal of Environmental Monitoring and Assessment*, Vol.13, 2011b, pp. 597–604.

[5]   D.R. Banjoo, P.K. Nelson, Improved ultrasonic extraction procedure for the determination of polycyclic aromatic hydrocarbons in sediments, *Journal of Chromatography A*, Vol.1066, 2005, pp. 9-18.

[6]   D.T. Sponza, R. Oztekin, Effect of sonication assisted by titanium dioxide and ferrous ions on Poly aromatic hydrocarbons (PAHs) and toxicity removals from a petrochemical industry wastewater in Turkey, *Journal of Chemical Technology and Biotechnology*, Vol.85, 2010, pp. 913–925

[7]   I. Quesada-Peñate, C. Julcour-Lebigue, U.-J. Jáuregui-Haza, A.-M. Wilhelm, D.H. Darie, Sonolysis of levodopa and paracetamol in aqueous solutions, *Ultrasonics Sonochemistry*, Vol.16, 2009, pp. 610-616.

[8]   M.R. Hoffmann, S.T. Martin, W. Choi, D.W. Bahnemann, Environmental applications of semiconductor photocatalysis, *Chemical Reviews,* Vol.95, 1995, pp. 69–96.

[9]   F. Sannino, P. Pernice, C. Imparato, A. Aronne, G. D'Errico, L. Minieri, M. Perfetti, D. Pirozzi, Hybrid TiO2-acetylacetonate amorphous gel-derived material with stably adsorbed superoxide radical active in oxidative degradation of organic pollutants, *RSC Advances,* Vol.5, 2015, pp. 93831–93839.

[10]   P. Zeng, Q. Zhang, X. Zhang, T. Peng, Graphite oxide–TiO2 nanocomposite and its efficient visible-light-driven photocatalytic hydrogen production, *Journal of Alloys and Compounds*, Vol.516, 2012, pp. 85–90.

[11]   A. Di Paola, E. Garcia-López, S. Ikeda, G. Marcı, B. Ohtani, L. Palmisano, Photocatalytic degradation of organic compounds in aqueous systems by transition metal doped polycrystalline TiO2, *Catalysis Today,* Vol.75, 2002, pp. 87–93.

[12]   K. Zhao, S.L. Zhao, J. Qi, H.J. Yin, C. Gao, A.M. Khattak, Y.J. Wu, A. Iqbal, L. Wu, Y. Gao, R.B. Yu, Z.Y. Tang, Cu2O clusters grown on TiO2 nanoplates as efficient photocatalysts for hydrogen generation, *Inorganic Chemistry Frontiers*, Vol.3, 2016, pp. 488–493.

[13]   L. Qu, Y. Liu, J.B. Baek, L. Dai, Nitrogen-doped graphene as efficient metal-free electrocatalyst for oxygen reduction in fuel cells, *ACS Nano*, Vol.4, 2010, pp. 1321–1326.

[14]   Y. Liang, Y. Li, H. Wang, J. Zhou, J. Wang, T. Regier, H. Dai, Co3O4 nanocrystals on graphene as a synergistic catalyst for oxygen reduction reaction, *Nature Materials,* Vol.10, 2011, pp. 780–786.

[15]   J. Guo, S. Zhu, Z. Chen, Y. Li, Z. Yu, Q. Liu, J. Li, C. Feng, D. Zhang, Sonochemical synthesis of TiO2 nanoparticles on graphene for use as photocatalyst, *Ultrasonics Sonochemistry*, Vol.18, 2011, pp. 1082–1090.

[16]   V. Stengl, J. Henych, P. Vomáčka, M. Slušná, Doping of TiO2-GO and TiO2-rGO with noble metals: synthesis, characterization and photocatalytic performance for azo dye discoloration, *Photochemistry and Photobiology*, Vol.89, 2013, pp. 1038–1046.

[17]   K.K. Turekian, K.H. Wedepohl, Distribution of the elements in some major units of the Earth's crust, *Geological Society of America Bulletin*, Vol.72, 1961, pp. 175.

[18]   R. Yousefi, F. Jamali-Sheini, M. Cheraghizade, S. Khosravi-Gandomani, A. Sáaedi, N.M. Huang, J.B. Wan, M. Azarang, Enhanced visible-light photocatalytic activity of strontium-doped zinc oxide nanoparticles, *Materials Science in Semiconductor Processing*, Vol.32, 2015, pp. 152.

[19]   L. Song, S. Zhang, B. Chen, A novel visible-light-sensitive strontium carbonate photocatalyst with high photocatalytic activity, *Catalysis Communications*, Vol.10, 2009, pp. 1565–1568.

[20]   H.R. Momenian, S. Gholamrezaei, M. Salavati-Niasari, B. Pedram, F. Mozaffar, D. Ghanbari, Sonochemical synthesis and photocatalytic properties of metal hydroxide and carbonate (M: Mg, Ca, Sr or Ba) nanoparticles, *Journal of Cluster Science*, Vol.24, 2013, pp. 1031–1042.

[21]   A. Márquezherrera, V. Ovandomedina, B. Castilloreyes, M. Zapatatorres, M. Meléndezlira, J. Gonzálezcastañeda, Facile synthesis of SrCO3-Sr(OH)2/PPy nanocomposite with enhanced photocatalytic activity under visible light, *Materials*, Vol.9, 2016, pp. 30.

[22]   P. Pichat, A brief overview of photocatalytic mechanisms and pathways in water, *Water Science and Technology*, Vol.55, 2007, pp. 167-173.

[23] G.V. Buxton, C.L. Greenstock, W.P. Helman, A.B. Ross, Critical review of rate constants for reactions of hydrated electrons, hydrogen atoms and hydroxyl radicals in aqueous solution, *Journal of Physical and Chemical Reference Data*, Vol.17, 1988, pp. 513-886.

[24] P.K.J. Robertson, L.A. Lawton, B. Münch, J. Rouzade, Destruction of cyanobacterial toxins by semiconductor photocatalysis, *Chemical Communications*, 1997, pp. 393-394.

[25] A.J. Feitz, T.D. Waite, G.J. Jones, B.H. Boyden, P.T. Orr, Photocatalytic degradation of the blue green algal toxin microcystin-LR in a natural organic-aqueous matrix, *Environmental Science and Technology*, Vol.33, 1999, pp. 243-249.

[26] L.A. Lawton, P.K.J. Robertson, B.J.P.A. Cornish, I.L. Marr, M. Jaspars, Processes influencing surface interaction and photocatalytic destruction of microcystins on titanium dioxide photocatalysts, *Journal of Catalysis*, Vol.213, 2003, pp. 109-113.

[27] M. Pelaez, A.A. de la Cruz, K. O'Shea, P. Falaras, D.D. Dionysiou, Effects of water parameters on the degradation of microcystin-LR under visible light-activated TiO 2 photocatalyst, *Water Research*, Vol.45, 2011, pp. 3787-3796.

[28] H. Choi, M.G. Antoniou, M. Pelaez, A.A. De La Cruz, J.A. Shoemaker, D.D. Dionysiou, Mesoporous nitrogen-doped TiO2 for the photocatalytic destruction of the cyanobacterial toxin microcystin-LR under visible light irradiation, *Environmental Science and Technology*, Vol.41, 2007, pp. 7530-7535.

[29] M. Pelaez, P. Falaras, V. Likodimos, A.G. Kontos, A.A. de la Cruz, K. O'shea, D.D. Dionysiou, Synthesis, structural characterization and evaluation of sol-gel-based NF-TiO2 films with visible lightphotoactivation for the removal of microcystin-LR, *Applied Catalysis B: Environmental*, Vol.99, 2010, pp. 378- 387.

[30] J. Andersen, C. Han, K. O'Shea, D.D. Dionysiou, Revealing the degradation intermediates and pathways of visible light-induced NF-TiO2 photocatalysis of microcystin-LR, *Applied Catalysis B: Environmental*, Vol.154-155, 2014, pp. 259-266.

[31] T. Fotiou, T.M. Triantis, T. Kaloudis, A. Hiskia, Evaluation of the photocatalytic activity of TiO2 based catalysts for the degradation and mineralization of cyanobacterial toxins and water off-odor compounds under UV-A, solar and visible light, *Chemical Engineering Journal*, Vol.261, 2015, pp. 17-26.

[32] T. Fotiou, T.M. Triantis, T. Kaloudis, K.E. O'Shea, D.D. Dionysiou, A. Hiskia, Assessment of the roles of reactive oxygen species in the UV and visible light photocatalytic degradation of cyanotoxins and water taste and odor compounds using C-TiO2, *Water Research*, Vol.90, 2016, pp. 52-61.

[33] M. Pelaez, P. Falaras, A.G. Kontos, A.A. De la Cruz, K. O'shea, P.S.M. Dunlop, J.A. Byrne, D.D. Dionysiou, A comparative study on the removal of cylindrospermopsin and microcystins from water with NF-TiO 2-P25 composite films with visible and UV-vis light photocatalytic activity, *Applied Catalysis B: Environmental*, Vol.121-122, 2012, pp. 30-39.

[34] T. Fotiou, T.M. Triantis, T. Kaloudis, L.M. Pastrana-Martínez, V. Likodimos, P. Falaras, A.M.T. Silva, A. Hiskia, Photocatalytic degradation of microcystin-LR and off-odor compounds in water under UV-A and solar light with a nanostructured photocatalyst based on reduced graphene oxide-TiO2 composite. Identification of intermediate products, *Industrial and Engineering Chemistry Research*, Vol.52, 2013, pp. 13991-14000.

[35] L. Eberson, Electron-Transfer Reactions in Organic Chemistry, *Advances in Physical Organic Chemistry*, Vol.18, 1982, pp. 79-185.

[36] P. Neta, R.E. Huie, A.B. Ross, Rate constants for reactions of inorganic radicals in aqueous solution, *Journal of Physical and Chemical Reference Data*, Vol.17, 1988, pp. 1027-1284.

[37] Y. Wang, C. Hong, Effect of hydrogen peroxide, periodate and persulfate on photocatalysis of 2- chlorobiphenyl in aqueous TiO2 suspensions, *Water Research*, Vol.33, 1999, pp. 2031-2036.

[38] O. Legrini, E. Oliveros, A.M. Braun, Photochemical processes for water treatment, *Chemical Reviews*, Vol.93, 1993, pp. 671-698.

[39] G.P. Anipsitakis, D.D. Dionysiou, Transition metal/UV-based advanced oxidation technologies for water decontamination, *Applied Catalysis B: Environmental*, Vol.54, 2004, pp. 155-163.

Rukiye Öztekin, Delia Teresa Sponza

[40] G.P. Anipsitakis, D.D. Dionysiou, M.A. Gonzalez, Cobalt-mediated activation of peroxymonosulfate and sulfate radical attack on phenolic compounds, Implications of chloride ions, *Environmental Science and Technology*, Vol.40, 2006, pp. 1000-1007.

[41] M.G. Antoniou, A.A. de la Cruz, D.D. Dionysiou, Degradation of microcystin-LR using sulfate radicals generated through photolysis, thermolysis and e- transfer mechanisms, *Applied Catalysis B: Environmental*, Vol.96, 2010a, pp. 290-298.

[42] M.G. Antoniou, A.A. De La Cruz, D.D. Dionysiou, Intermediates and reaction pathways from the degradation of microcystin-LR with sulfate radicals, *Environmental Science and Technology*, Vol.44, 2010b, pp. 7238-7244.

[43] X. He, A.A. de la Cruz, K.E. O'Shea, D.D. Dionysiou, Kinetics and mechanisms of cylindrospermopsin destruction by sulfate radical-based advanced oxidation processes, *Water Research*, Vol.63, 2014, pp. 168-178

[44] X. He, A.A. de la Cruz, A. Hiskia, T. Kaloudis, K. O'Shea, D.D. Dionysiou, Destruction of microcystins (cyanotoxins) by UV-254 nm-based direct photolysis and advanced oxidation processes (AOPs): Influence of variable amino acids on the degradation kinetics and reaction mechanisms, *Water Research*, Vol.74, 2015, pp. 227-238.

[45] M. Antonopoulou, I.K. Konstantinou, Effect of oxidants in the photocatalytic degradation of DEET under simulated solar irradiation in aqueous TiO2 suspensions, *Global NEST Journal*, Vol.16, 2014, pp. 507-515.

[46] V. Augugliaro, C. Baiocchi, A.B. Prevot, E. García-López, V. Loddo, S. Malato, G. Marcí, L. Palmisano, M. Pazzi, E. Pramauro, Azo-dyes photocatalytic degradation in aqueous suspension of TiO2 under solar irradiation, *Chemosphere*, Vol.49, 2002, pp. 1223-1230.

[47] M. Saquib, M. Muneer, TiO2/mediated photocatalytic degradation of a triphenylmethane dye (gentian violet), in aqueous suspensions, *Dyes and Pigments*, Vol.56, 2003, pp. 37-49.

[48] W.S. Hummers Jr., R.E. Offeman, Preparation of graphitic oxide, *Journal of the American Chemical Society*, Vol.80, 1958, pp. 1339.

[49] Z. Xu, Q. Li, S. Gao, J.K. Shang, As(III) removal by hydrous titanium dioxide prepared from one-step hydrolysis of aqueous TiCl4 solution, *Water Research*, Vol.44, 2010, pp. 5713–5721

[50] J. Fu, Y. Gong, Z. Cai, S.E. O'Reilly, D. Zhao, Mechanistic investigation into sunlight-facilitated photodegradation of pyrene in seawater with oil dispersants, *Marine Pollution Bulletin*, Vol.114, 2017, pp. 751–758.

[51] M.E. Lindsey, M.A. Tarr, Quantitation of hydroxyl radical during Fenton oxidation following a single addition of iron and peroxide, *Chemosphere*, Vol.41, 2000, pp. 409-417.

[52] R.B. Baird, A.D. Eaton, E.W. Rice, Standard Methods for the Examination of Water and Wastewater. E.W. Rice (editor), 23rd. Edition, American Public Health Association (APHA), American Water Works Association (AWWA), Water Environment Federation (WEF). American Public Health Association 800 I Street, NW Washington DC: 20001-3770, USA, January 1, 2017; ISBN-13: 978-0875532875; ISBN-10: 087553287X.

[53] J.H. Zar, Biostatistical Analysis. Prentice-Hall, Englewood Cliffs. 1984.

[54] Statgraphics Centurion XV, sofware , StatPoint Inc, Statgraphics Centurion XV, Herndon, VA, USA, 2005.

[55] G.Z. Kyzas, N.A. Travlou, E.A. Deliyanni, The role of chitosan as nanofiller of graphite oxide for the removal of toxic mercury ions, *Colloids and Surfaces B: Biointerfaces*, Vol.113, 2014, pp. 467–476. [

[56] M.A. Alavi, A. Morsali, Syntheses and characterization of Sr(OH)2 and SrCO3 nanostructures by ultrasonic method, *Ultrasonics Sonochemistry*, Vol.17, 2010, pp. 132–138.

[57] K. Thamaphat, P. Limsuwan, B. Ngotawornchai, Phase characterization of TiO2 powder by XRD and TEM Kasetsart, *Journal of Natural Sciences*, Vol.42, 2008, pp. 357–361.

[58] S.-T. Huang, W.W. Lee, J.-L. Chang, W.-S. Huang, S.-Y. Chou, C.-C. Chen, Hydrothermal synthesis of SrTiO3 nanocubes: characterization, photocatalytic activities, and degradation pathway, *Journal of the Taiwan Institute of Chemical Engineers*, Vol.E 45, 2014, pp. 1927–1936.

[59] K. Wysmulek, J. Sar, P. Osewski, K. Orlinski, K. Kolodziejak, A. Trenczek-Zajac, M. Radecka, D.A. Pawlak, A SrTiO3-TiO2 eutectic composite as a stable photoanode material for photoelectrochemical hydrogen

production, *Applied Catalysis B: Environmental*, Vol.206, 2017, pp. 538–546.

[60] Z. He, X.-Y. Sun, X. Gu, Electrospinning fabrication of SrTiO3:Er3+ nanofibers and their applications of upconversion properties, *Ceramics International*, Vol.43, 2017, pp. 7378–7382.

[61] S. Lowell, Introduction to powder surface area, John Wiley & Sons, 1979.

[62] A.G. Chakinala, P.R. Gogate, R. Chand, D.H. Bremner, R. Molina, A.E. Burgess, Intensification of oxidation capacity using chloroalkanes as additives in hydrodynamic and acoustic cavitation reactors, *Ultrasonics Sonochemistry*, Vol.15, 2008, pp. 164–170.

[63] J. Fu, G.Z. Kyzasc, Z. Cai, E.A. Deliyanni, W. Liu, D. Zhao, Photocatalytic degradation of phenanthrene by graphite oxide-TiO2-Sr (OH)2/SrCO3 nanocomposite under solar irradiation: Effects of water quality parameters and predictive modeling, *Chemical Engineering Journal*, Vol.335, 2018, pp. 290–300.

[63] J. Chen, W.J.G.M. Peijnenburg, X. Quan, S. Chen, D. Martens, K.W. Schramm, A. Kettrup, Is it possible to develop a QSPR model for direct photolysis half-lives of PAHs under irradiation of sunlight? *Environmental Pollution*, Vol.114, 2001, pp. 137–143.

[64] T. Kanagaraj, S. Thiripuranthagan, Photocatalytic activities of novel SrTiO3–BiOBr heterojunction catalysts towards the degradation of reactive dyes, *Applied Catalysis B Environmental*, Vol.207, 2017, pp. 218–232.

[65] R.P. Cavalcante, R.F. Dantas, B. Bayarri, O. González, J. Giménez, S. Esplugas, A. Machulek Jr., Photocatalytic mechanism of metoprolol oxidation by photocatalysts TiO2 and TiO2 doped with 5% B: primary active species and intermediates, *Applied Catalysis B: Environmental*, Vol.194, 2016, pp. 111–122.

[66] G.P. Anipsitakis, D.D. Dionysiou, Degradation of organic contaminants in water with sulfate radicals generated by the conjunction of peroxymonosulfate with cobalt, *Environmental Science and Technology*, Vol.37, 2003, pp. 4790-4797.

[67] I.K. Konstantinou, T.A. Albanis, TiO2-assisted photocatalytic degradation of azo dyes in aqueous solution: Kinetic and mechanistic investigations: A review, *Applied Catalysis B Environmental*, Vol.49, 2004, pp. 1-14.

[68] M.G. Antoniou, P.A. Nicolaou, J.A. Shoemaker, A.A. de la Cruz, D.D. Dionysiou, Impact of the morphological properties of thin TiO2 photocatalytic films on the detoxification of water contaminated with the cyanotoxin, microcystin-LR, *Applied Catalysis B: Environmental*, Vol.91, 2009, pp. 165-173.

Contribution of Individual Authors to the Creation of a Scientific Article (Ghostwriting Policy)
Post-Dr. Rukiye Öztekin and Prof. Dr. Delia Teresa Sponza took an active role in every stage of the preparation of this article.

APPENDIX

Table 2: Physical and chemical properties of the PAHs in petrochemical industry wastewater studied in this work

PAHs	CAS-No	MF	MW (g/mol)	T_M (ºC)	T_B (ºC)	S_W (25ºC) (mg/l)	V_P (25ºC) (mm Hg)	H (25ºC) (atm m^3/mol)	log K_{OA} (25ºC)	log K_{OW}	SORC
ACL	208-96-8	$C_{12}H_8$	152	93	280	16.1	6.68E-03	1.14E-04	6.34	3.94	23.56E+10
CRB	86-74-8	$C_{12}H_9N$	167	246	355	1.8	7.50E-07	1.16E-06	8.03	3.72	24.67E+10
BkF	207-08-9	$C_{20}H_{12}$	252	217	480	0.0008	9.70E-10	5.84E-08	11.37	6.11	0.45E+8
BaP	50-32-8	$C_{20}H_{12}$	252	177	495	0.00162	5.49E-09	4.57E-07	11.56	6.13	0.32 E+8

Acenaphthylene (ACL), Carbazole (CRB), Benzo[*k*]fluoranthene (BkF), Benzo[*a*]pyrene (BaP)

MF: Molecular Formula, MW: Molecular weight, T_M: Melting point (ºC), T_B: Boiling point(ºC), S_W: Solubility in water (mg/l), V_P: Vapor pressure (mm Hg), H: Henry's law constant (atm m^3/mol), log K_{OA}: Octanol-air coefficient, log K_{OW}: Octanol-water coefficient, SORC: second-order reaction rate constants (mg/l.s).
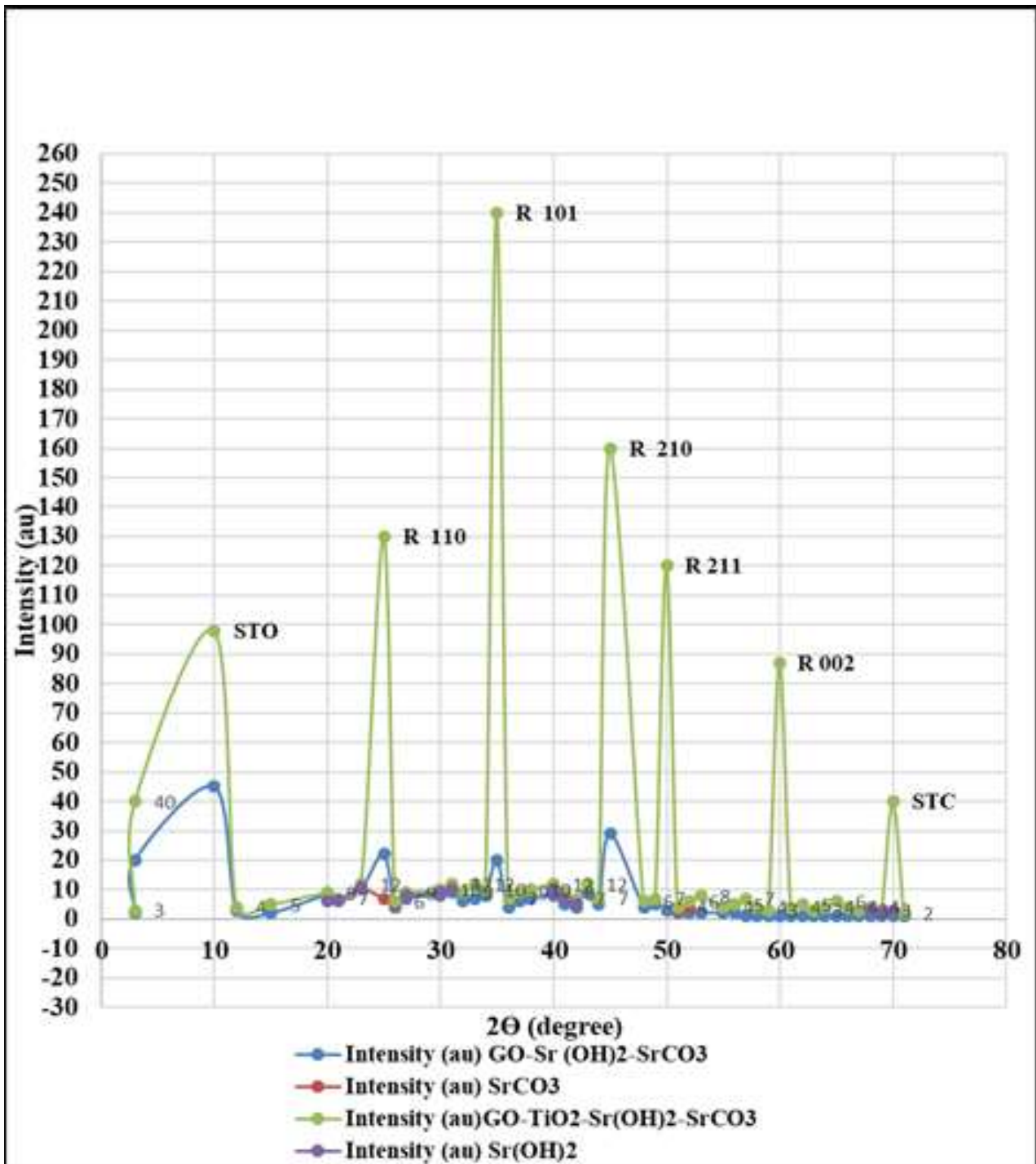
Rukiye Öztekin, Delia Teresa Sponza

Figure 1: XRD patterns of GO-Sr(OH)₂/SrCO₃ and GO-TiO₂-Sr(OH)₂/SrCO₃ nanocomposites in petrochemical industry wastewater

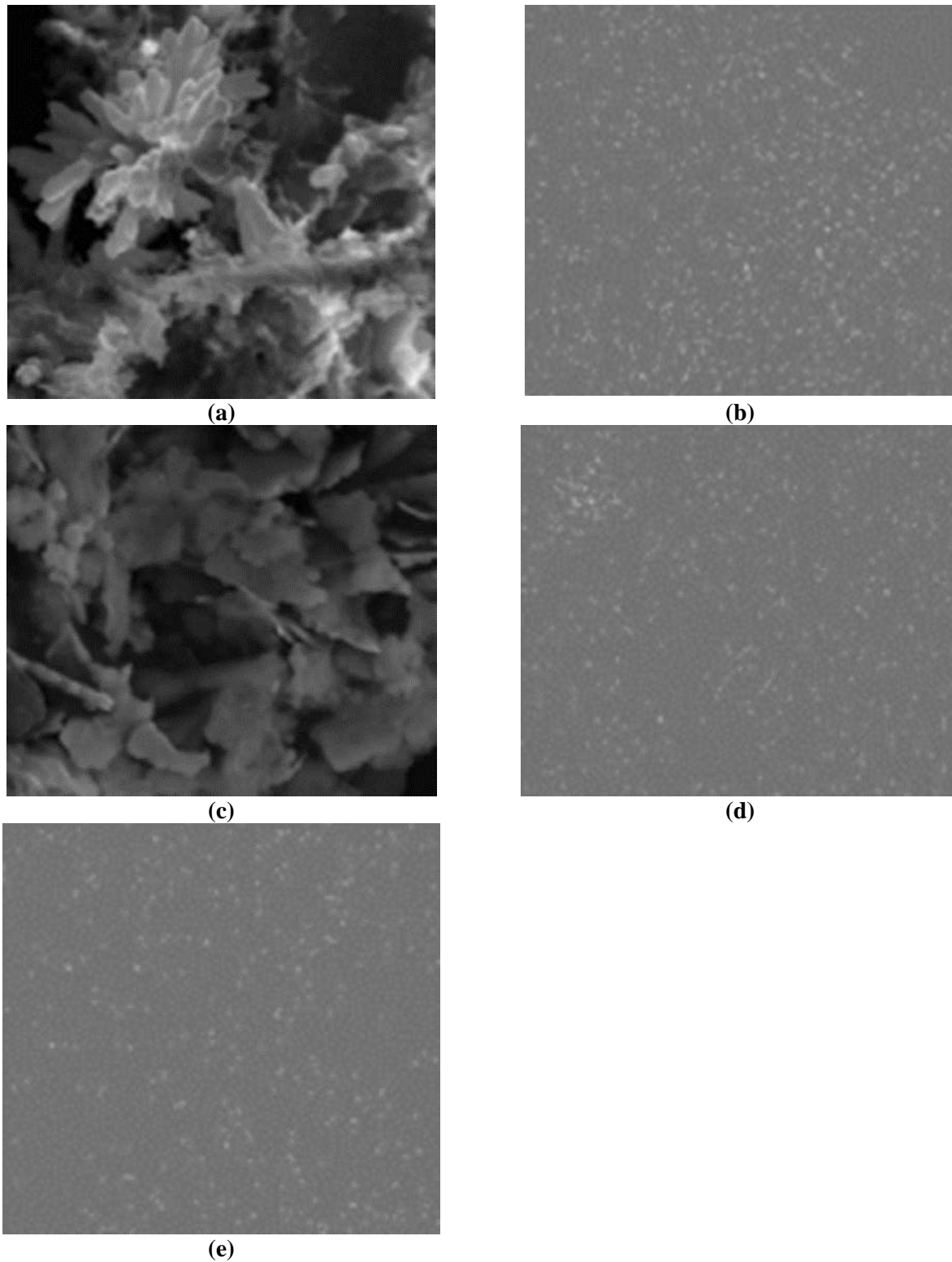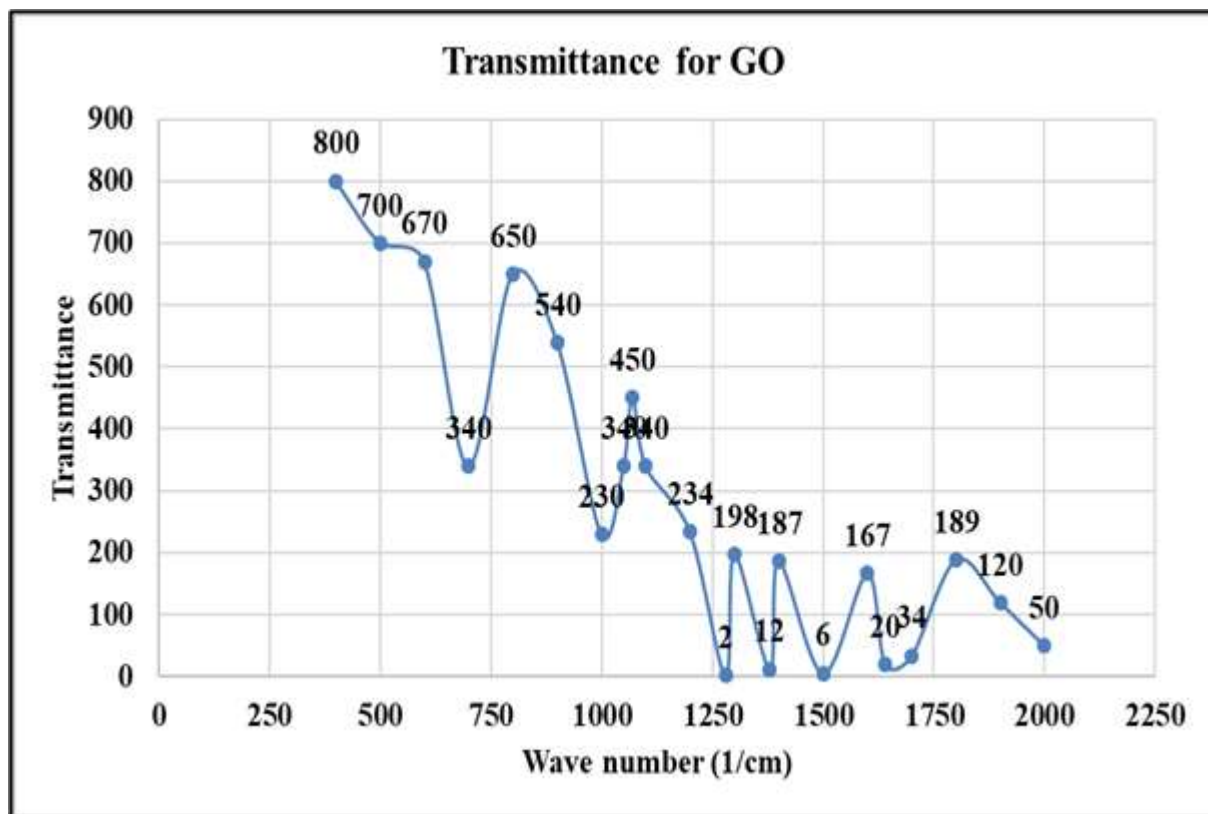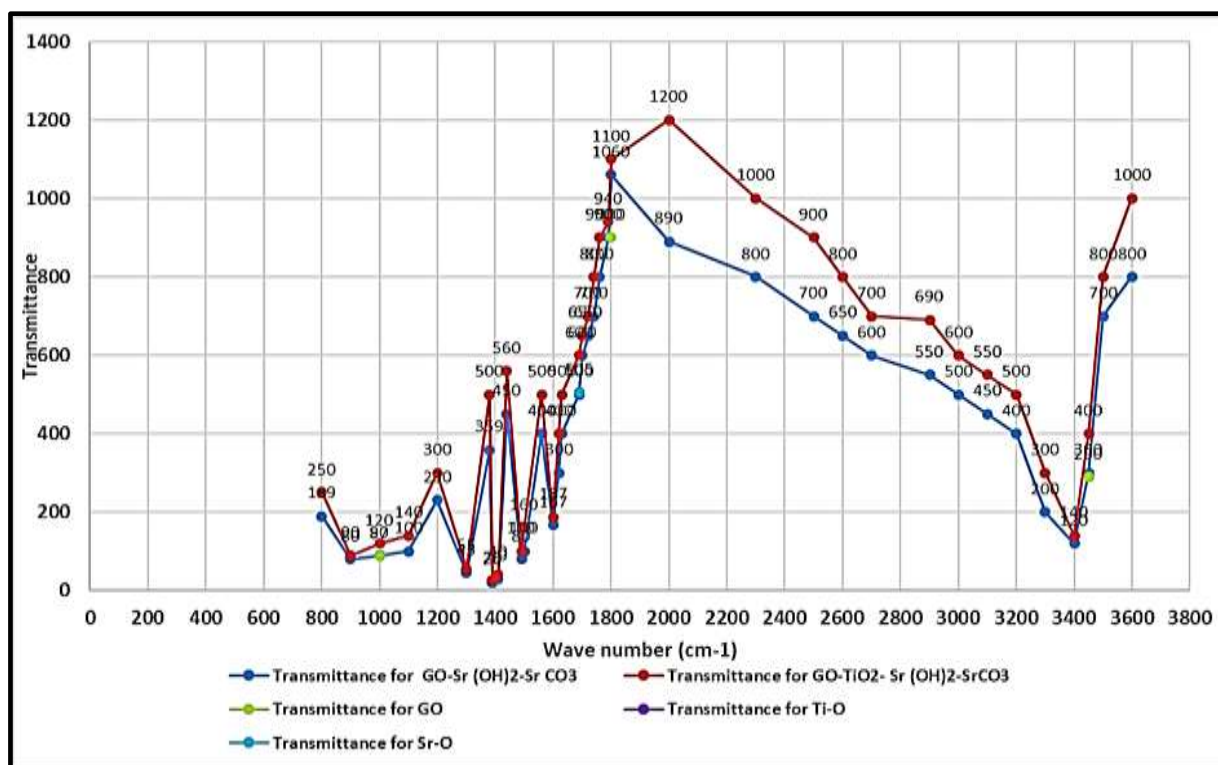**Figure 2:** SEM images of **(a)** GO-Sr(OH)$_2$/SrCO$_3$, **(b)** Sr distribution EDX map with GO-Sr(OH)$_2$/SrCO$_3$, **(c)** GO-TiO$_2$-Sr(OH)$_2$/SrCO$_3$, **(d)** Sr distribution EDX map with GO-TiO$_2$-Sr(OH)$_2$/SrCO$_3$ and **(e)** Ti distribution EDX map in petrochemical industry wastewater.
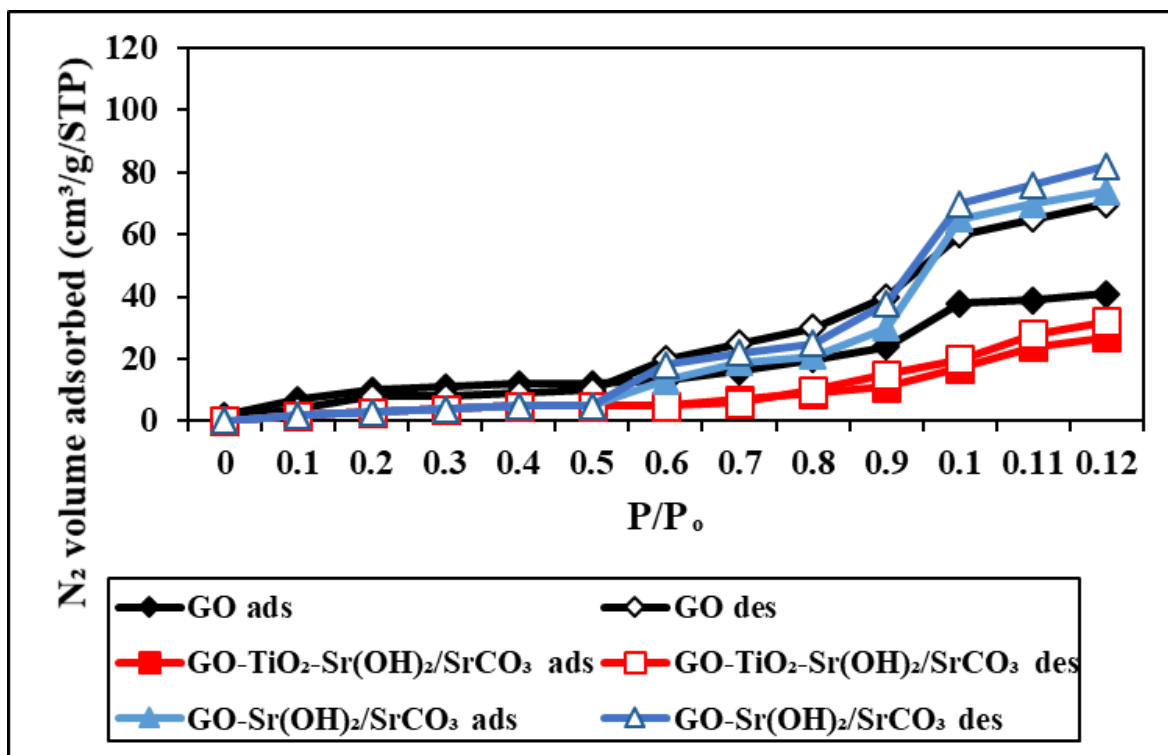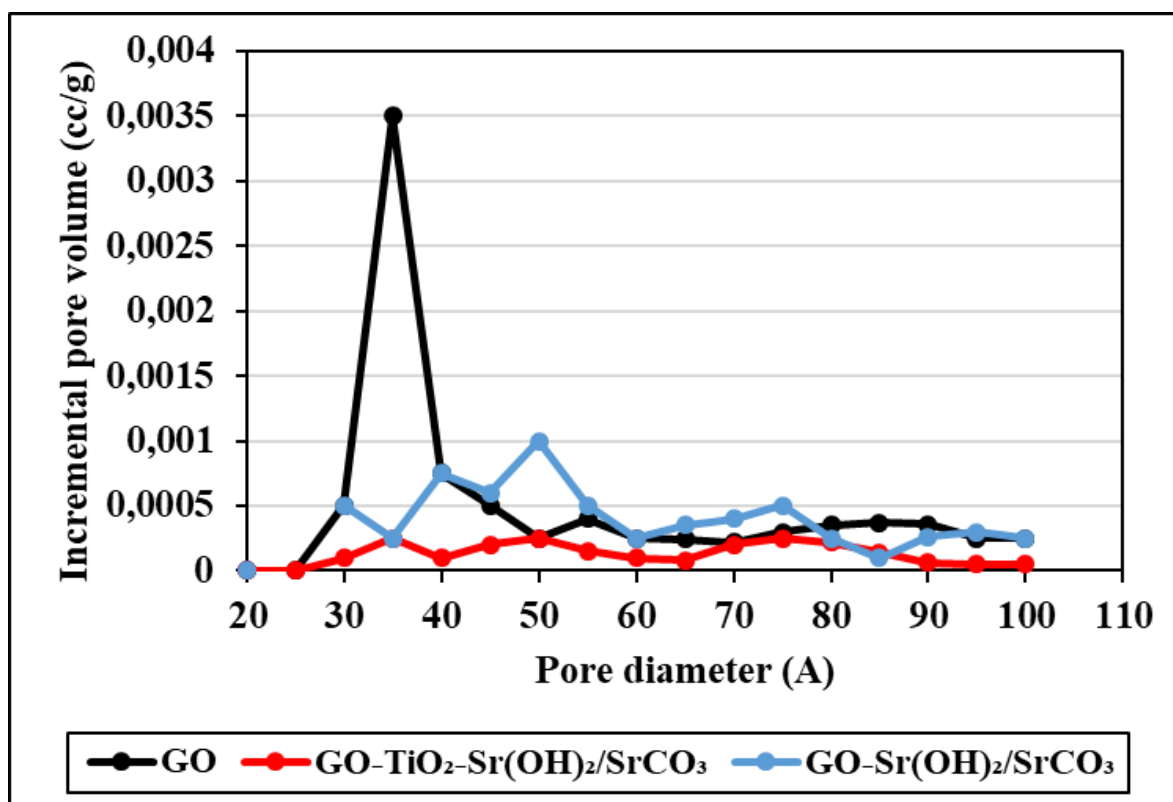
(a)

(b)

Figure 3: FTIR spectra of **(a)** GO and **(b)** GO-Sr(OH)$_2$/SrCO$_3$ versus GO-TiO$_2$-Sr(OH)$_2$/SrCO$_3$ nanocomposites in petrochemical industry wastewater.

(a)

(b)

Figure 4: (a) Nitrogen adsorption-desorption isotherms and **(b)** pore size distribution of GO, GO-Sr $(OH)_2/SrCO_3$ and GO-TiO$_2$-Sr(OH)$_2$/SrCO$_3$ in petrochemical industry wastewater.

Table 3: Effect of increasing experimental parameters on photocatalytic degradation of hydrophobic PAHs in a petrochemical industry wastewater under sun light irradiation process, at 100 mW/cm^2 sun light intensity, at pH=7.0 and at 22°C, respectively (n=3, mean values).

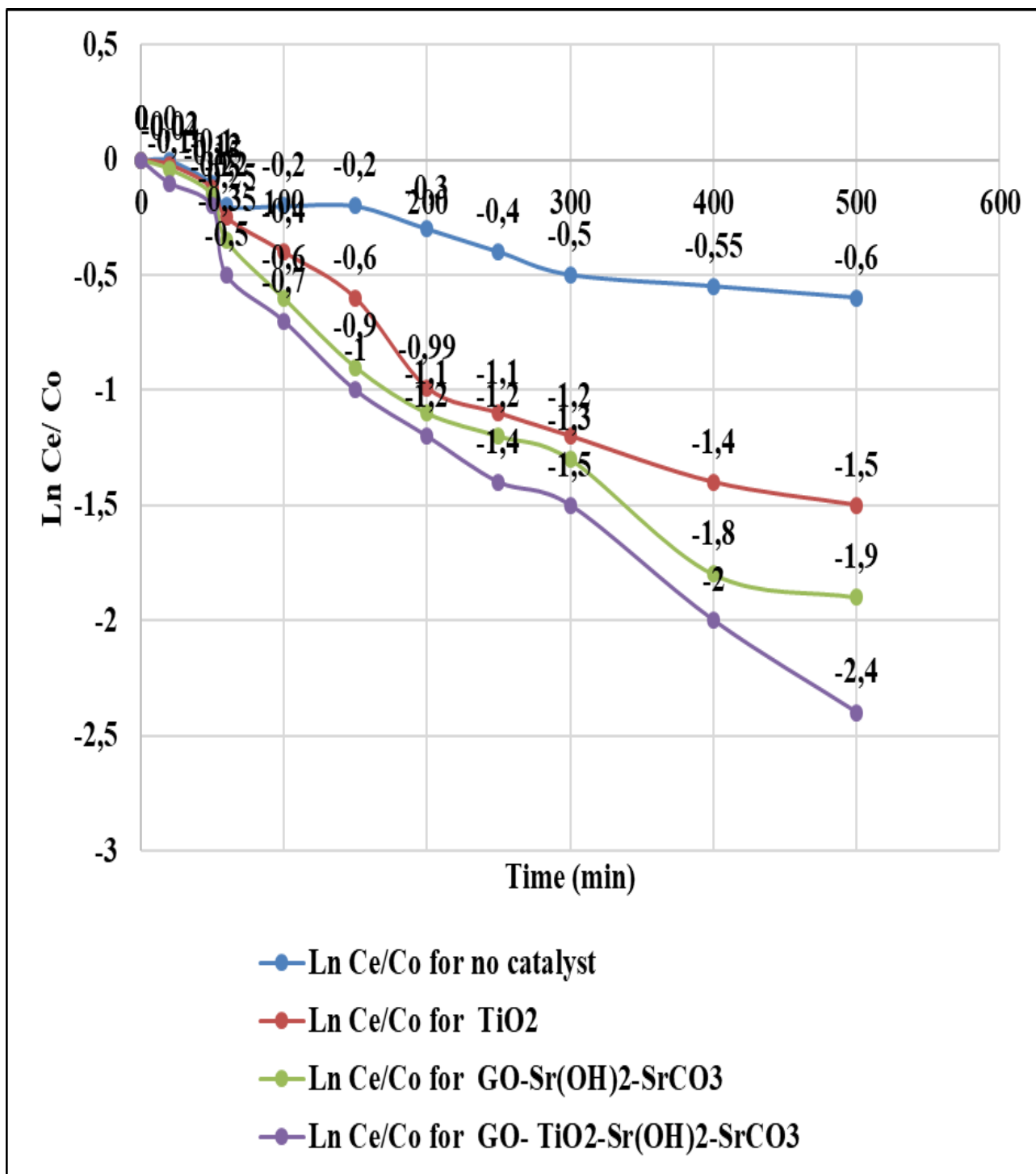| Set	Parameters	Hydrophobic PAHs removals (%)			
		Less hydrophobic		More hydrophobic	
		ACL	CRB	BaP	BkF
1	**GO nanoparticle concentrations (mg/l)**				
	2	54	56	59	58
	4	71	73	70	69
	8	87	87	85	84
2	**TiO$_2$ nanoparticle concentrations (mg/l)**				
	1	59	57	64	75
	3	63	66	77	81
	6	76	78	83	86
	9	89	90	91	92
3	**GO-TiO$_2$-Sr(OH)$_2$/SrCO$_3$ nanocomposite concentrations (mg/l)**				
	1	76	75	80	92
	2	89	84	86	97
	4	97	98	98	99
4	**Sun light irradiation times (min)**				
	30	56	61	60	65
	120	65	68	65	66
	240	74	76	72	79
	360	81	80	84	84
5	**Photocatalytic powers (W)**				
	10	56	62	67	69
	50	69	70	78	74
	100	84	86	88	89

Rukiye Öztekin, Delia Teresa Sponza

Figure 5: Photocatalytic degradation of PAHs in petrochemical industry wastewater by various synthesized catalysts, at 100 mW/cm^2 sun light intensity, at 250 ml solution volume, at 1 mg/l initial PAHs concentration, at 50 mg/l catalyst dosage, at 360 min sun light irradiation time, at pH=7.0 and at 22°C, respectively.
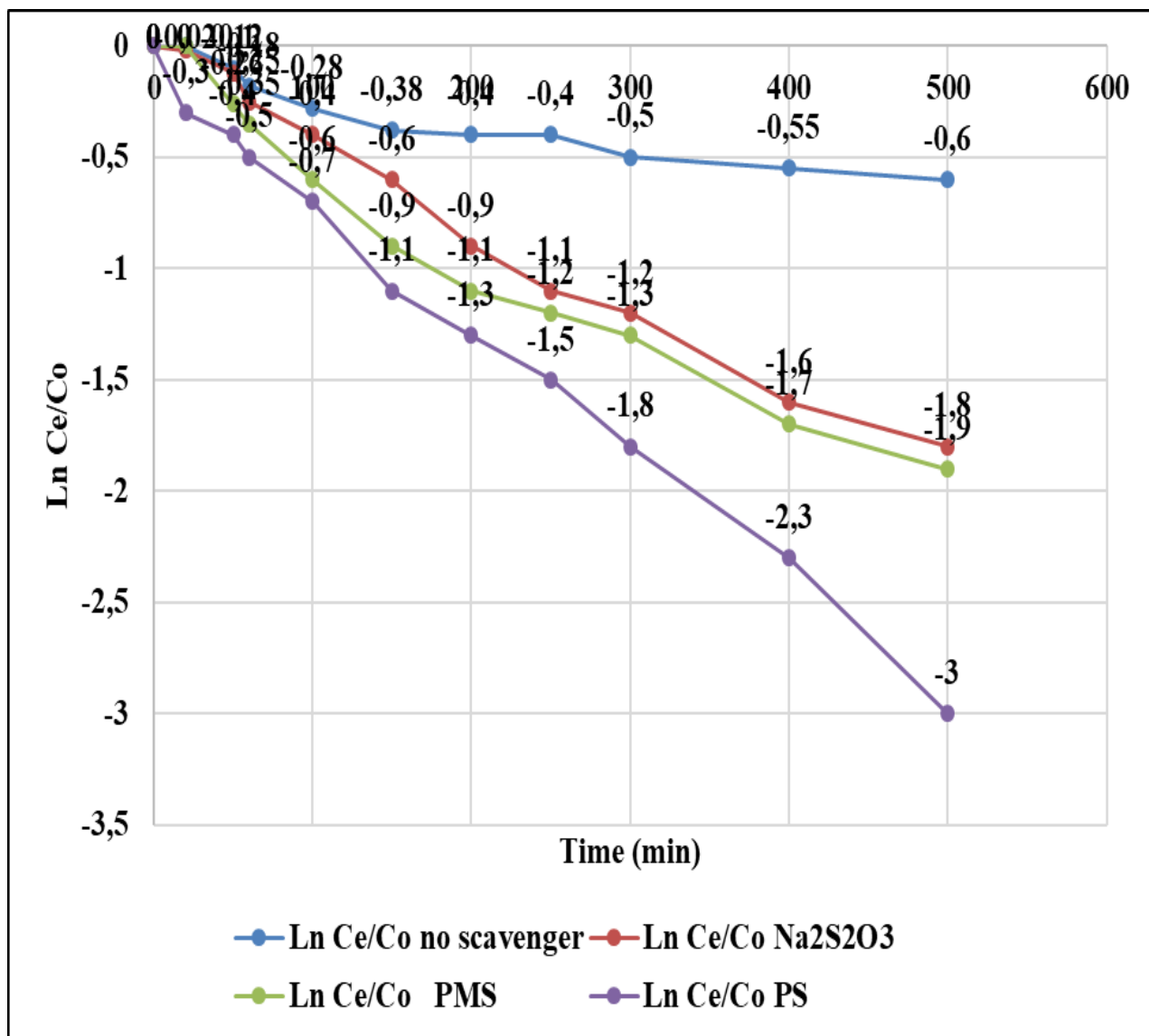
Figure 6: Photocatalytic degradation of PAHs in petrochemical industry wastewater by $GOTiO_2$-$Sr(OH)_2/SrCO_3$ in the various radical scavengers, at 100 mW/cm^2 sun light intensity, at 250 ml solution volume, at 1 mg/l initial PAHs concentration, at 50 mg/l catalyst dosage, at 200 mg/l TBA dosage, at 200 mg/l NaN_3 dosage, at 200 mg/l BQ dosage and at 4000 U/ml CAT dosage, at pH=7.0±0.2, T=22±1°C, respectively.

Table 7: Effect of sun light irradiation times during photocatalytic degradation process in petrochemical industry wastewater on the acute toxicity (EC_{50}) removal efficiencies at different operational conditions at pH=7.0 and at 22°C (n=3, mean values).

Sets	IAT		PDA at 22°C (Control)			Operational conditions								
						GO			TiO_2			GO-TiO_2-Sr(OH)$_2$/SrCO$_3$		
	EC_{50} t=0	ATR_i	SLIT [a]	EC_{50}	ATR	GO [b]	EC_{50} t=360	ATR_e	$TiO2$ [c]	EC_{50} t=360	ATR_e	GO-TiO_2-Sr(OH)$_2$/SrCO$_3$ [d]	EC_{50} t=360	ATR_e
1	342.56	98	30	359.04	2.01	2	631.05	99.99	1	484.67	67	1	590.56	97.00
2	342.56	98	120	364.78	6.23	4	604.67	90.00	3	545.56	78	2	626.56	99.00
3	342.56	98	240	377.67	8.34	8	540.78	76.99	6	587.45	94	4	630.45	99.94
4	342.56	98	360	380.12	10.01				9	504.67	70			

IAT: Initial acute toxicity; a: sun light irradiation times (min); b: GO concentration (mg/l); c: TiO_2 nanoparticle concentrations (mg/l); d: GO-TiO_2-Sr(OH)$_2$/SrCO$_3$ nanocomposite concentration (mg/l); PDA: Photocatalytic degradation alone without additives (Control); EC_{50} t=0 : Initial acute toxicity before photocatalytic degradation (mg/l); ATR_i: Initial inhibition percentage before photocatalytic degradation; EC_{50} : Acute toxicity after photocatalytic degradation in control versus sun light irradiation time (mg/l); ATR: Acute toxicity removal (%) in control versus sun light irradiation time; ATR_e: Acute toxicity removal (%) after 360 min sun light irradiation time; EC_{50} t=360 : acute toxicity after 360 min sun light irradiation time (mg/l).